https://doi.org/10.1093/plcell/koad151 THE PLANT CELL 2023: 35: 3303–3324

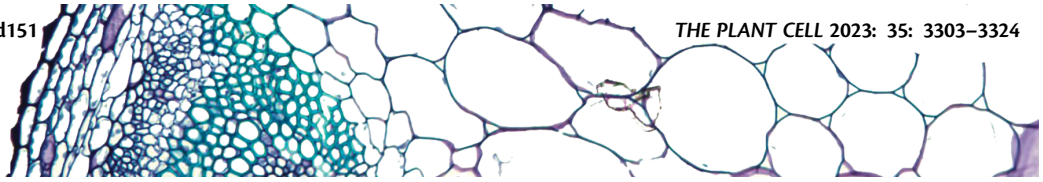

Research Article

# The P-body component DECAPPING5 and the floral repressor SISTER OF FCA regulate *FLOWERING LOCUS C* transcription in Arabidopsis

**Wanyi Wang, Chuanhong Wang, Yunhe Wang, Jing Ma, Tengyue Wang, Zhen Tao, Peipei Liu, Shuai Li, Yuanyuan Hu, Aiju Gu, Hui Wang, Chunhong Qiu and Peijin Li**

The National Engineering Lab of Crop Stress Resistance Breeding, School of Life Sciences, Anhui Agricultural University, Hefei 230036, China

*Author for correspondence: Peijin.li@ahau.edu.cn
†These authors contributed equally to this work.
‡Senior author.
The author responsible for distribution of materials integral to the findings presented in this article in accordance with the policy in the Instructions for Authors (https://academic.oup.com/plcell/pages/General-Instructions) is: Peijin Li (Peijin.li@ahau.edu.cn).

## Abstract

Flowering is the transition from vegetative to reproductive growth and is critical for plant adaptation and reproduction. *FLOWERING LOCUS C* (*FLC*) plays a central role in flowering time control, and dissecting its regulation mechanism provides essential information for crop improvement. Here, we report that DECAPPING5 (DCP5), a component of processing bodies (P-bodies), regulates *FLC* transcription and flowering time in Arabidopsis (*Arabidopsis thaliana*). DCP5 and its interacting partner SISTER OF FCA (SSF) undergo liquid–liquid phase separation (LLPS) that is mediated by their prion-like domains (PrDs). Enhancing or attenuating the LLPS of both proteins using transgenic methods greatly affects their ability to regulate *FLC* and flowering time. DCP5 regulates *FLC* transcription by modulating RNA polymerase II enrichment at the *FLC* locus. DCP5 requires SSF for *FLC* regulation, and loss of SSF or its PrD disrupts DCP5 function. Our results reveal that DCP5 interacts with SSF, and the nuclear DCP5–SSF complex regulates *FLC* expression at the transcriptional level.

## Introduction

Flowering is essential for plant reproduction and adaptation. Extensive natural variation at the *FRIGIDA* (*FRI*) and *FLOWERING LOCUS C* (*FLC*) loci is a major factor determining the winter-annual (late flowering) or rapid-cycling (early flowering) growth habits of the cruciferous species Arabidopsis (*Arabidopsis thaliana*) (Johanson et al. 2000; Shindo et al. 2006). While FRI induces *FLC* transcription, proteins including FLOWERING CONTROL LOCUS A (FCA), FLOWERING LOCUS PA, FLOWERING LOCUS D, and FY form the autonomous pathway and antagonize FRI function to repress *FLC* expression (Macknight et al. 1997; Schomburg et al. 2001; Simpson et al. 2003; Crevillen and Dean 2011). We recently identified *SISTER OF FCA* (*SSF*) through genome-wide association studies and revealed that it promotes *FLC* transcription and delays flowering (Wang et al. 2020). Arabidopsis accessions harbor either one of two haplotypes for *SSF*, one of which results in an amino acid change that modulates the interaction between SSF and CULLIN1 and manipulates RNA polymerase II (Pol II) enrichment at the *FLC* locus, leading to differential *FLC* transcription and flowering time (Wang et al. 2020). Nevertheless, the precise mechanism of SSF function in regulating *FLC* requires further investigation.

In addition to conventional membrane-bound organelles, cells also contain several types of membraneless and

Received December 16, 2022. Accepted April 30, 2023. Advance access publication May 23, 2023

## IN A NUTSHELL

**Background:** Typical organelles such as mitochondria and chloroplasts are surrounded by membranes. However, eukaryotic cells also contain organelles that lack membranes. For example, P-bodies consist of cytoplasmic condensates and act in mRNA processing, including mRNA decapping, mRNA degradation, deadenylation, RNA-mediated post-transcriptional gene silencing, and nonsense-mediated decay P-bodies are conserved across eukaryotes. In plants, P-bodies and their constituent proteins undergo liquid–liquid phase separation (LLPS). In LLPS, proteins and nucleic acids form a dense, separate phase that looks like droplets of liquid. However, it is unclear where the LLPS occurs and how it is related to important biological processes such as flowering time, which affects plant growth, development, and seed yield.

**Question:** What is the function of the essential P-body component DECAPPING5 (DCP5)? How does DCP5 affect flowering time?

**Findings:** We applied protein coimmunoprecipitation combined with mass spectrometry (IP-MS) analysis on the flowering regulator SISTER OF FCA (SSF), and identified the SSF-interacting protein DCP5. A knockdown mutation of *DCP5* (*dcp5-1*) affected the expression of the floral repressor *FLOWERING LOCUS C* (*FLC*) and resulted in late flowering compared to the wild type. The *dcp5-1* mutation led to more RNA polymerase II enrichment at the *FLC* locus and higher *FLC* transcription. *FLC* mRNA stability was not affected in *dcp5-1*. Moreover, we showed that DCP5 was recruited to *FLC* genomic regions by SSF. More importantly, we discovered that the regulation of *FLC* by the DCP5–SSF complex depended on LLPS.

**Next steps:** To better understand the role of the DCP5–SSF complex in the cotranscriptional regulation of *FLC*, we will identify additional proteins that interact with SSF or DCP5 for flowering time regulation in Arabidopsis.

noncovalent compartments composed of proteins or RNA molecules that are thought to play critical roles in ubiquitous biological pathways such as RNA metabolism, translation, and signal transduction (Banani et al. 2017). These compartments, also called biomolecular condensates, refer to the spatial concentration of biomolecules into speckles/spots, as observed by microscopy (Boija et al. 2018; Emenecker et al. 2020), such as stress-induced granules, processing bodies (P-bodies), nucleoli, Cajal bodies, and dicing bodies (D-bodies) (Collier et al. 2006; Kroschwald et al. 2015; Luo et al. 2018; Xie et al. 2020). Some RNA-binding proteins have been reported to contain intrinsically disordered domains of low complexity that are essential for proteins undergoing liquid–liquid phase separation (LLPS) either alone or in the presence of RNA (Fang et al. 2019; Ji et al. 2019). To date, how and where most phase-separation events take place remains elusive, and the biological function of most examples of cellular phase separation is unclear (Emenecker et al. 2020).

P-bodies consist of cytoplasmic condensates and contribute to multiple steps in mature mRNA processing, including mRNA decapping, mRNA degradation, deadenylation, RNA-mediated post-transcriptional gene silencing, and nonsense-mediated decay (Maldonado-Bonilla 2014; Schütz et al. 2017). P-bodies are conserved across eukaryotes and display liquid droplet properties that are enhanced by the addition of RNA (Schütz et al. 2017). DECAPPING1 (DCP1), DCP2, DCP5, and VARICOSE are major components of the P-body in plants. DCP5 shows similarity to human RNA-associated protein 55 (Xu and Chua 2012) and is required for pre-mRNA decapping, inhibition of mRNA translation, and P-body formation (Xu and Chua 2009).

In Arabidopsis, a protein complex comprising SM-LIKE1 (LSM1) and LSM7 in the cytoplasm is involved in P-body formation, mRNA decapping and decay, playing a critical role in Arabidopsis development. Interestingly, the LSM2–LSM8 complex localizes in the nucleus, regulating *U6* small nuclear RNA stabilization and pre-mRNA splicing (Perea-Resa et al. 2012). Moreover, DCP5 affects the localization of DCP1 and DCP2 in plants (Xu and Chua 2009; Jang et al. 2019), enabling selective translation for optimal development of Arabidopsis seedlings (Jang et al. 2019). DCP5 also works together with LSM1 to evade translational repression during cauliflower mosaic virus (CaMV) infection (Hoffmann et al. 2022).

Here, we show that SSF interacts with DCP5 in the nucleus to cotranscriptionally regulate *FLC* expression. Our data suggest that both proteins undergo LLPS, which is required for their ability to regulate *FLC*, with DCP5 enhancing SSF LLPS. We also demonstrate that SSF recruits DCP5 to *FLC* chromatin to repress *FLC* transcription.

## Results

### SSF interacts with DCP5, a component of the P-body complex

We previously showed that SSF regulated *FLC* transcription and flowering in Arabidopsis (Wang et al. 2020). To further dissect the molecular mechanism of SSF, we identified its interacting partners by protein pull-down assays using *ssf-2 proSSF:SSF–GFP* transgenic plants (Wang et al. 2020), followed by mass spectrometry analysis. From these experiments, we identified a candidate SSF-interacting protein: DCP5 (At1g26110), a component essential for the formation of the P-body (Xu and Chua 2009; Jang et al. 2019)

(Supplemental Data Set 1). To validate this interaction, we performed yeast two-hybrid (Y2H) assays with SSF fused to the yeast (*Saccharomyces cerevisiae*) GAL4 DNA-binding domain (BD-SSF) and DCP5 fused to the GAL4 activation domain (AD-DCP5). Only cells cotransformed with both constructs grew on selective medium, while either construct cotransformed with the corresponding empty vector did not. Furthermore, truncated SSF variants (SSFΔPrD and $SSF^{WW}$) did not interact with DCP5 (Fig. 1A; Supplemental Fig. S1).

We performed luciferase (LUC) complementation imaging (LCI) assays in *Nicotiana benthamiana* leaf cells and bimolecular fluorescence complementation (BiFC) assays in Arabidopsis protoplasts. For LCI assays, we coinfiltrated *N. benthamiana* leaves with constructs encoding SSF-nLUC (SSF fused to the N-terminal half of LUC), SSFΔPrD-nLUC, $SSF^{WW}$-nLUC and cLUC-DCP5 (DCP5 fused to the C-terminal half of LUC). We observed strong LUC activity when *SSF-nLUC* and *cLUC-DCP5* were coexpressed, but not for *SSFΔPrD-nLUC* and *cLUC-DCP5* or $SSF^{WW}$*-nLUC* and *cLUC-DCP5*, consistent with the reconstitution of LUC due to protein-protein interaction (Fig. 1B). For BiFC assays, we transiently transfected Arabidopsis protoplasts with plasmids encoding nYFP-SSF (SSF fused to the N-terminal half of yellow fluorescent protein) and cYFP-DCP5 (DCP5 fused to the C-terminal half of yellow fluorescent protein) and detected YFP fluorescence, supporting the interaction of SSF with DCP5 (Fig. 1C). SSF–GFP predominantly localized in the nucleus, while we detected DCP5–mCherry in the nucleus and the cytosol, with clear colocalization of the two proteins in the nucleus (Fig. 1D).

DCP5 interacted with SSF in in vitro protein pull-down assays using recombinant GFP–SSF and mCherry–DCP5, when GFP–SSF and mCherry–DCP5 mixture solution was pulled down by magnetic beads coupled with anti-GFP antibodies and detected with an anti-mCherry antibody (Fig. 1E). We also conducted in vivo protein coimmunoprecipitation (Co-IP) assays using transgenic Arabidopsis plants harboring *proSSF:SSF–GFP* and *proDCP5:DCP5–FLAG* transgenes, which confirmed the interaction between SSF and DCP5 when using anti-GFP antibodies (Fig. 1F). FCA is homologous to SSF, prompting us to hypothesize that it may also interact with DCP5. Accordingly, we tested the DCP5–FCA interaction by performing Y2H and BiFC assays. In contrast to our expectation, FCA failed to interact with SSF or DCP5 in yeast or in Arabidopsis protoplasts (Supplemental Fig. S2).

To explore which domain in DCP5 plays a major role in the SSF–DCP5 interaction, we carried out interaction analysis using truncated DCP5 variants. DCP5 contains four major domains: one Like-Sm domain (LSM), one Phe-Asp-Phe (FDF), and two Arg-Gly-Gly domains (RGG). We generated several truncated DCP5 proteins for interaction assays: truncated C-terminal domain (DCP5ΔC), truncated N-terminal LSM domain (DCP5ΔN), and both N- and C-terminal domains deleted (DCP5M) (Fig. 1G). We first checked the localization of DCP5ΔC, DCP5ΔN, and DCP5M as GFP fusions to their C termini in *N. benthamiana* leaf cells: we determined that DCP5ΔC, DCP5ΔN, and DCP5M localize to the nucleus and cytosol (Supplemental Fig. S3, A to D). The BiFC assays showed that both DCP5ΔC and DCP5ΔN can interact with SSF in Arabidopsis protoplasts, while DCP5M could not (Fig. 1H). We further divided DCP5 into DCP5N and DCP5C, and observed that both fragments can interact with SSF in BiFC assays. DCP5N and DCP5C localized in the nucleus and cytoplasm (Fig. 1H; Supplemental Fig. S3, E and F). These results indicate that both the N- and C-terminal domains of DCP5 can interact with SSF.

## DCP5 regulates flowering time in Arabidopsis by downregulating *FLC* expression

We performed genetic characterization of *DCP5* with the *dcp5-1* knockdown mutant, which harbors a T-DNA insertion in the 3′ untranslated region (3′ UTR) of *DCP5* (Supplemental Fig. S4, A and B). *DCP5* transcript levels were about one-third those in wild-type Col-0 (Fig. 2A). Moreover, the *dcp5-1* mutant flowered later when grown under a long-day photoperiod (Fig. 2B) and accumulated higher levels of spliced (mature) and unspliced (nascent) *FLC* transcripts (Fig. 2, C and D). To verify the late-flowering phenotype of *dcp5-1*, we generated stable transgenic plants carrying a *proDCP5:DCP5–GFP* complementation transgene in the *dcp5-1* mutant background. The transgene restored *DCP5* transcripts to levels similar to wild-type (Fig. 2A), rescued the delayed flowering time phenotype of the *dcp5-1* mutant (Fig. 2B), and reduced *FLC* transcript levels back to Col-0 level (Fig. 2, C and D).

Given that unspliced *FLC* was increased in the *dcp5-1* mutant (Fig. 2D), we suspected a role for DCP5 in the nucleus (Fig. 1D). To confirm that DCP5 exists in the nucleus as seen by confocal imaging (Fig. 2E), we extracted proteins from *dcp5-1 proDCP5:DCP5–FLAG* transgenic Arabidopsis seedlings and separated soluble proteins into nuclear and cytosolic fractions for immunoblot analysis. We only detected the nuclear protein Histone H3 in the nuclear fraction, while only the cytosolic fraction accumulated actin, indicating that these fractions lack detectable contamination (Zavaliev et al. 2020). Consistent with the DCP5–GFP localization in the nucleus (Fig. 2E), we obtained a signal for DCP5–FLAG in both the nuclear and cytosolic fractions with an anti-FLAG antibody (Fig. 2F).

We performed chromatin immunoprecipitation (ChIP) assays to evaluate RNA Pol II occupancy at the *FLC* locus in the *dcp5-1* mutant. Significantly more RNA Pol II accumulated in the *dcp5-1* mutant over the entire *FLC* genomic region than in the wild-type control (Col-0), but the enrichment was significantly lower in the *dcp5-1 proDCP5:DCP5–GFP* transgenic complementation plants relative to *dcp5-1* (Fig. 2, G and H). In addition, we did not detect a significant difference in *FLC* mRNA stability between *dcp5-1* and wild-type Col-0, and we obtained similar results for *ssf-2* (Supplemental Fig. S4C). These results indicate that DCP5 can regulate flowering time by modulating *FLC* transcription.

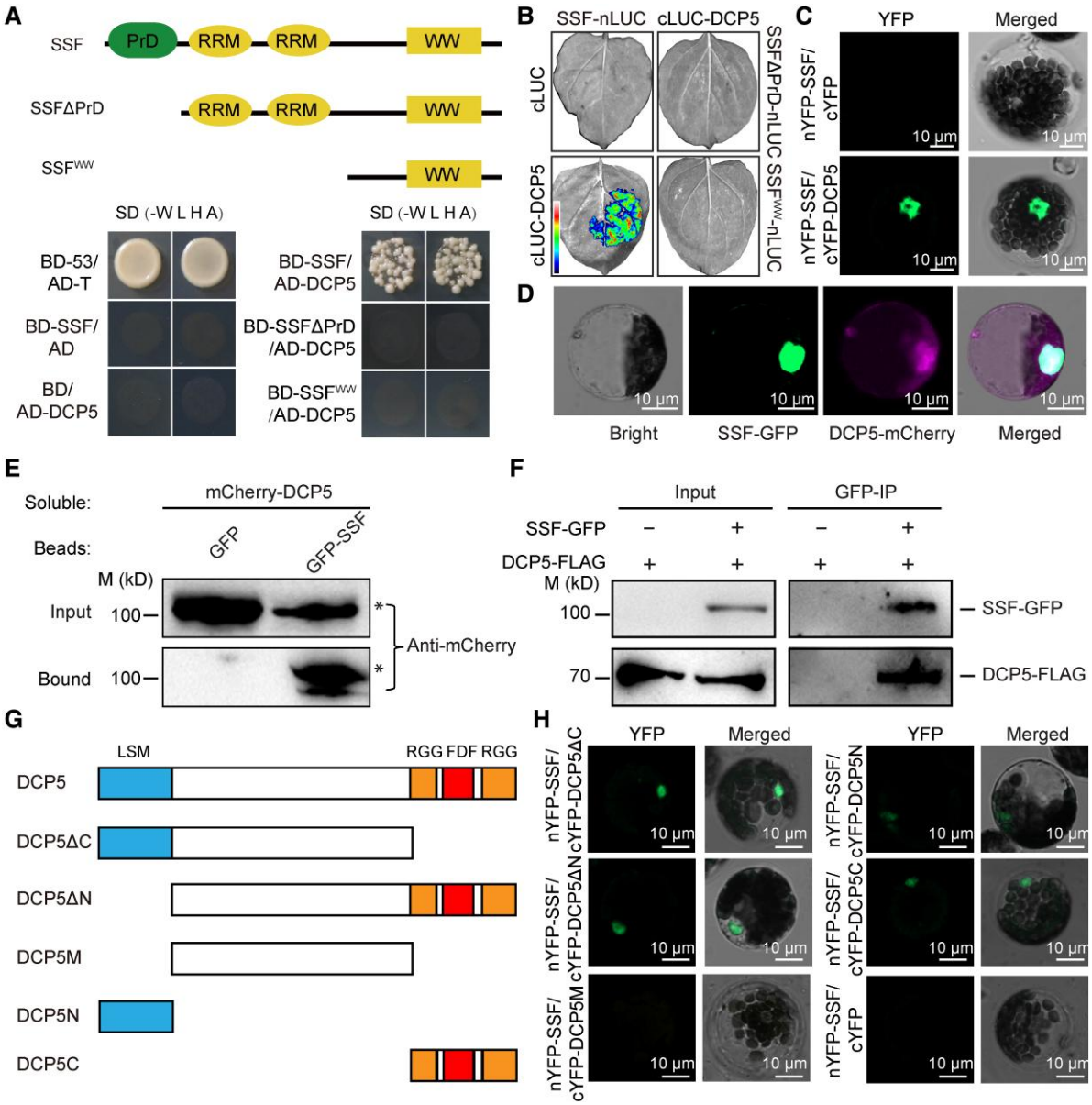


**Figure 1.** SSF interacts with the P-body component DCP5 in vitro and in vivo. **A)** The prion-like domain (PrD) is a key domain mediating the interaction between SSF and DCP5 in yeast (*Saccharomyces cerevisiae*) cells. The interaction between P53 and T was used as a positive control. pGBKT7 (empty bait vector; BD) with DCP5 and pGADT7 (empty prey vector; AD) with SSF were used as negative controls. **B** and **C)** Luciferase (LUC) complementation imaging (LCI) (**B**) and bimolecular fluorescence complementation (BiFC) assays (**C**) show that SSF interacts with DCP5 in *Nicotiana benthamiana* cells (**B**) and in Arabidopsis protoplast cells (**C**). **D)** SSF–GFP and DCP5–mCherry colocalize in the nuclei of Arabidopsis protoplasts. **E)** Protein pull-down assays show that SSF interacts with DCP5 in vitro. mCherry fused to DCP5 (mCherry–DCP5) was tested for binding to GFP fused to SSF (GFP–SSF). GFP alone was used as a negative control in the pull-down assays. M, molecular weight of protein marker. **F)** Coimmunoprecipitation (Co-IP) assay using stable transgenic plants to detect the association of SSF–GFP with DCP5–FLAG. The *SSF–GFP* transgenic line was crossed to a *DCP5–FLAG* transgenic line. F3 generation plants were used for Co-IP. **G)** Schematic diagram of the different domains of DCP5. **H)** BiFC showing that SSF interacts with DCP5C and DCP5N, but not with DCP5M, in Arabidopsis protoplasts. Scale bars, 10 μm. All experiments were performed at least 3 times, and representative results are shown.

## DCP5 binding to *FLC* chromatin is SSF-dependent

The *ssf-2* mutant flowered earlier than wild-type Col-0, while *dcp5-1* flowered later (Fig. 3A). To elucidate the genetic relationship between *SSF* and *DCP5*, we generated the *ssf-2 dcp5-1* double mutant by crossing. The *ssf-2 dcp5-1* double mutant flowered almost at the same time as the *ssf-2* single mutant (Fig. 3, A and B). In agreement with this result, *FLC* transcript levels in *ssf-2 dcp5-1* were comparable to those in *ssf-2*, and much lower than in *dcp5-1* (Fig. 3, C and D), indicating that *ssf-2* can suppress the high *FLC* transcript levels and late flowering seen in *dcp5-1*. To confirm this result, we obtained transgenic Arabidopsis lines constitutively overexpressing *DCP5*

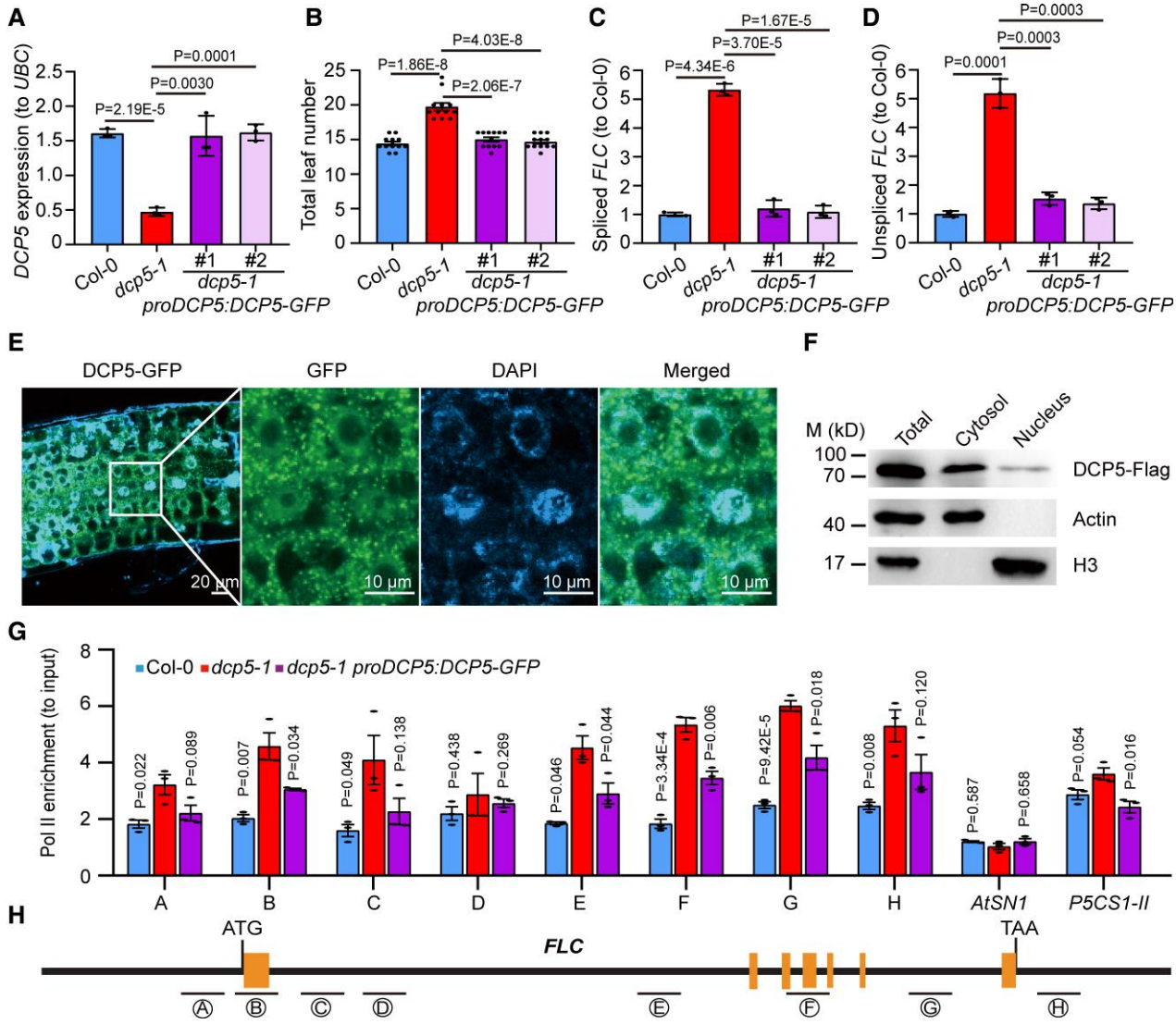


**Figure 2.** DCP5 downregulates *FLC* expression in Arabidopsis. **A)** *DCP5* expression was restored to wild-type levels in *dcp5-1 proDCP5:DCP5–GFP* transgenic plants (lines #1 and #2), compared to that in wild-type Col-0 and *dcp5-1*. **B)** Flowering time (as total leaf number) of the indicated genotypes. **C** and **D)** Spliced (**C**) and unspliced (**D**) *FLC* transcript levels are lower in *dcp5-1 proDCP5:DCP5–GFP* transgenic plants compared to *dcp5-1*. The gene expression values from RT-qPCR were normalized to Col-0. **E)** Subcellular localization analysis of DCP5–GFP. 4′,6-diamidino-2-phenylindole staining was used to mark nuclei. Scale bars, 20 or 10 μm. **F)** Immunoblot analysis indicating that DCP5–FLAG exists in the nucleus and cytosol. Histone H3 and actin specifically accumulate in the nucleus and cytosol, respectively, and were used as indicators for the separation of nuclear and cytosolic fractions. M, molecular weight of protein marker. **G)** RNA Polymerase II (Pol II) is more highly enriched in the *dcp5-1* mutant, compared to that in wild-type Col-0. The *P*-values illustrate significance level relative to *dcp5-1*. *AtSN1*, negative control; *P5CS1-II*, positive control. **H)** Schematic diagram of the *FLC* locus. The boxes with yellow color, exons; horizontal lines, introns. The ChIP-qPCR primer positions are shown as letters in the figure. In (**A**, **C**, **D**), *UBC* was used as an internal control for qPCR, data are means of three independent experiments ± standard deviation (SD) ($n = 50$ seedlings per replicate). In (**B**), data are means of 12 plants ± standard error of the mean (SEM). In (**G**), data are means of three independent experiments ± SEM (3 g of seedlings per replicate). Significant differences were determined using Student's *t*-test. All experiments were performed at least 3 times, and representative results are shown.

under the control of the CaMV 35S promoter in the Col-0 background (*DCP5*-OE) and crossed them to *ssf-2* to obtain *ssf-2 DCP5*-OE plants.

The flowering time of the *DCP5*-OE lines was significantly earlier than that of Col-0 (Fig. 3E; Supplemental Fig. S5A). Consistent with this result, *FLC* transcript levels in *DCP5*-OE were lower than in Col-0 (Fig. 3, F and G), while *DCP5* transcript levels in *DCP5*-OE were higher than in Col-0 (Supplemental Fig. S5B). By contrast, we observed no significant difference in flowering time or *FLC* transcript levels between *ssf-2 DCP5*-OE and *ssf-2* (Fig. 3, H to J; Supplemental Fig. S5C), although the expression of *DCP5* in *ssf-2 DCP5*-OE was much higher than in *ssf-2* (Supplemental Fig. S5D), suggesting that SSF is required for DCP5 to repress *FLC* expression.

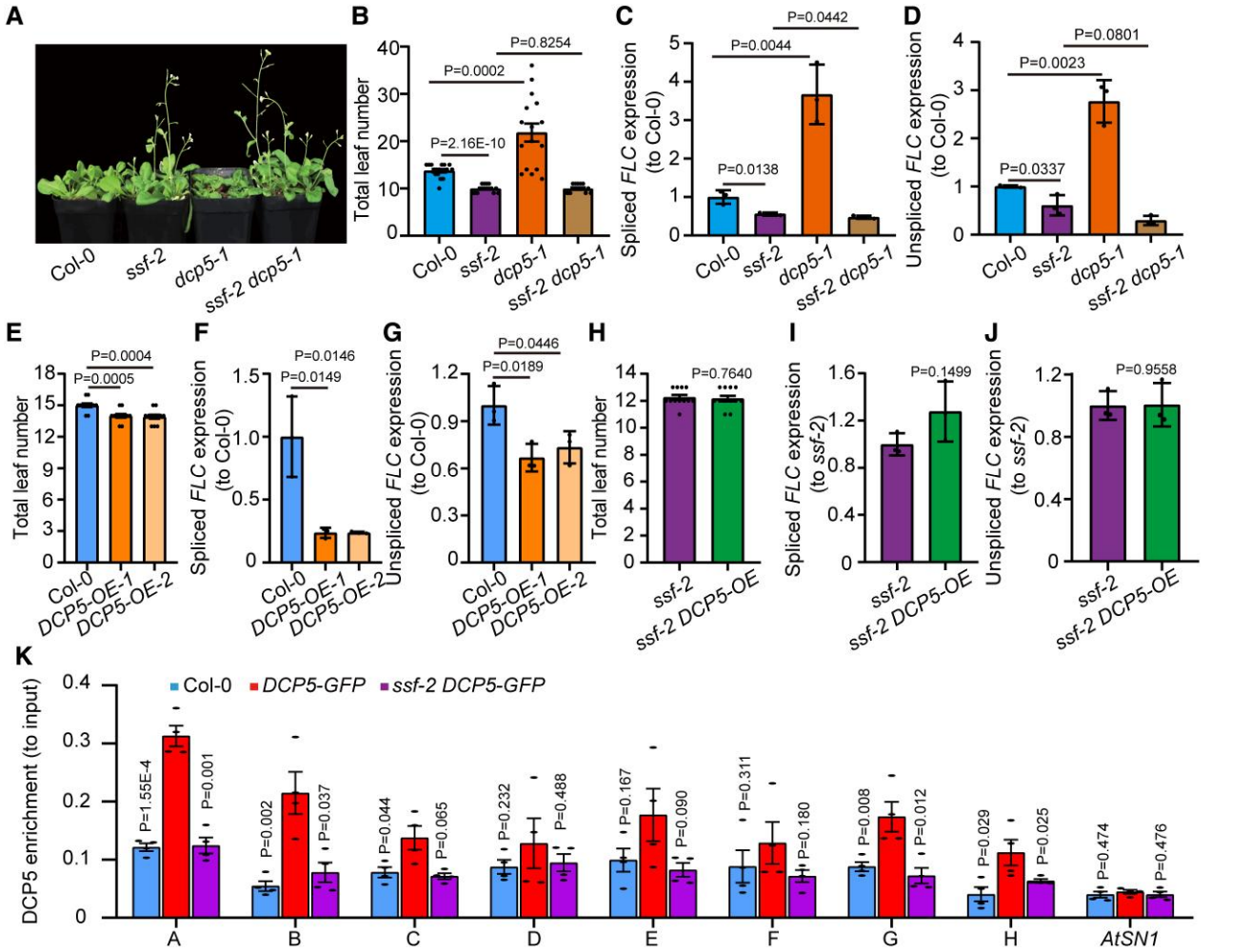


**Figure 3.** SSF recruits DCP5 to repress *FLC* transcription and flowering. **A)** Phenotype of Col-0, *ssf-2*, *dcp5-1* and *ssf-2 dcp5-1*. Note the *ssf-2 dcp5-1* plants flower at the same time as *ssf-2*. **B)** Flowering time (as total leaf number) of Col-0, *ssf-2*, *dcp5-1* and *ssf-2 dcp5-1*. **C** and **D)** Levels of spliced (**C**) and unspliced (**D**) *FLC* transcripts in Col-0, *ssf-2*, *dcp5-1* and *ssf-2 dcp5-1*. **E)** Total leaf number of Col-0 and *DCP5*-OE (Col-0 background) overexpression lines. **F** and **G)** Levels of spliced (**F**) and unspliced (**G**) *FLC* transcripts in Col-0 and *DCP5*-OE. **H)** Total leaf number of *ssf-2* and *ssf-2 DCP5*-OE Arabidopsis plants. **I** and **J)** Expression of spliced (**I**) and unspliced (**J**) *FLC* transcripts in *ssf-2* and *ssf-2 DCP5*-OE ($n = 3$). **K)** DCP5 enrichment at *FLC* genomic regions is dependent on SSF. The ChIP-qPCR primer positions are as indicated in the diagram in Fig. 2H. The *P*-values illustrate statistical significance relative to *DCP5–GFP*. *AtSN1*: negative control. In (**B**, **E**, and **H**), data are means of 12 plants ± SEM. In (**C**, **D**, **F**, **G**, **I**, and **J**), *UBC* was used as an internal control for qPCR, data are means of three independent experiments ± SD ($n = 50$ seedlings per replicate). In (**K**), data are means of four independent experiments ± SEM (3 g of seedlings per replicate). Significant differences were determined using Student's *t*-test. All experiments were performed at least 3 times, and representative results are shown.

We also discovered that DCP5 binds to multiple regions of the *FLC* locus, as evidenced by ChIP-qPCR assays. Notably, DCP5 binding to the *FLC* locus was SSF-dependent, as DCP5 enrichment was lost when the ChIP assay was performed in *ssf-2 proDCP5:DCP5–GFP* (Figs. 3K and 2H). Taken together, these data suggest that SSF is essential for DCP5 to bind to *FLC* chromatin.

## SSF undergoes phase separation

*SSF* encodes a putative RNA-binding protein (RBP) with two RNA recognition motifs and one WW domain (Figs. 1A and 4A). Fang et al. (2019) reported that the SSF homolog FCA has a prion-like domain (PrD), which affects its function. Therefore, we speculated that SSF may also have a PrD, although the biological roles of SSF and FCA are not the same (Wang et al. 2020). The prion-like amino acid composition (PLAAC) prediction tool detected one candidate PrD in SSF spanning amino acids 7 to 83, while the Database of Disordered Protein Prediction (D2P2) program identified three disordered regions in SSF, one of which partially overlapped with the PrD (Figs. 1A and 4A). We then determined the subcellular localization of SSF tagged with GFP (SSF–-GFP) in *ssf-2 proSSF:SSF–GFP* transgenic plants. Previous work established that the SSF–GFP fusion protein is functional (Wang et al. 2020). SSF–GFP was nonuniformly distributed in the nucleus, with clear differences from the GFP control (Fig. 4B).

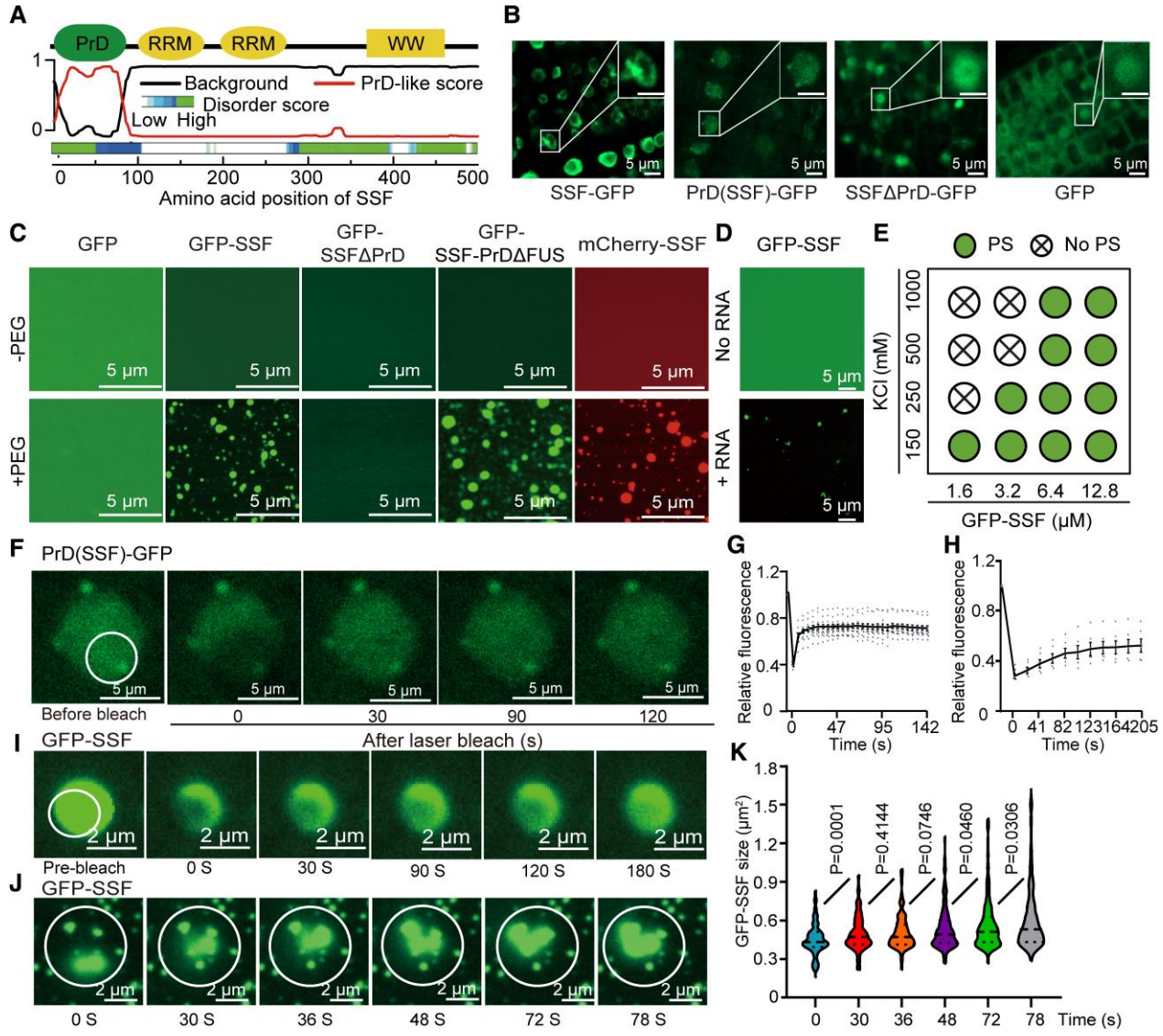


**Figure 4.** The flowering time regulator SSF shows phase separation. **A)** Schematic diagram of the SSF protein. Top, the four domains of SSF are shown. Prion-like domain (PrD). RRM, RNA recognition motif. WW, Trp-Trp domain; middle, PrD score (0 to 1) is displayed compared to the background (analyzed by "prion-like amino acid composition", PLAAC; http://plaac.wi.mit.edu/); bottom, disordered regions of SSF as predicted by D2P2 (http://d2p2.pro/). **B)** SSF–GFP and PrD(SSF)–GFP form fluorescent speckles in the roots of transgenic Arabidopsis seedlings, whereas SSFΔPrD–GFP and GFP do not. PrD(SSF), the PrD of SSF. SSFΔPrD, SSF without its PrD. Scale bars, 5 μm. **C)** In vitro phase-separation assays of GFP, GFP–SSF, GFP–SSFΔPrD, GFP–SSF–PrDΔFUS, and mCherry–SSF with 10% (w/v) PEG4000 treatment for 10 min. PrDΔFUS, PrD was replaced by FUS. Scale bars, 5 μm. Note: the deletion of PrD abolished the phase-separation capacity of SSF. **D)** Phase separation of GFP–SSF was tested in the presence of total RNA extracted from Arabidopsis seedlings. Scale bars, 5 μm. **E)** Dynamic LLPS of GFP–SSF with different concentrations of KCl and recombinant GFP–SSF. **F)** PrD(SSF)–GFP forms multiple speckles in the nuclei of transgenic Arabidopsis seedlings. Scale bars, 5 μm. **G)** The relative GFP fluorescence of PrD(SSF)–GFP in the nuclei of transgenic Arabidopsis plants recovers after photobleaching. Data are means of the fluorescence values from 15 seedlings ± SEM. The images were taken every 3 s over 142 s to document fluorescence recovery, each time point was normalized to the value before photobleaching. **H** and **I)** GFP–SSF can recover after photobleaching. Scale bars, 2 μm. Data are means of the fluorescence values from six droplets ± SEM. The images were taken every 20 s over 205 s to document fluorescence recovery, each time point was normalized to the value before photobleaching. **J** and **K)** GFP–SSF droplets can fuse and form larger droplets. Scale bars, 2 μm ($n = 210$ droplets). The circles in (**F** and **I**) indicate the photobleached regions for recovery analysis. All experiments were performed at least 3 times, and representative results are shown.

To gain a better view of the spatial organization of SSF in the nucleus, we performed AX microscopy with NSPARC (Nikon Spatial Array Confocal; a confocal-based super resolution microscope) to overcome the optical diffraction limit and capture SSF localization. We established that SSF–GFP in the nucleus shows a spot-like pattern (Supplemental Fig. S6A). When we transiently expressed *SSF–GFP* driven by 35S promoter in *N. benthamiana* leaf epidermal cells, SSF–GFP aggregated into multiple large,

round foci (0.1 to 9.95 μm$^2$ in size), which was distinct from the GFP control (Supplemental Fig. S6, D and E). To test the role of the SSF PrD, we generated stable transgenic lines expressing *PrD(SSF)–GFP* under the native *SSF* promoter in Arabidopsis. PrD(SSF)–GFP formed multiple fluorescent foci in Arabidopsis root cells (Fig. 4B) and distributed nonuniformly in *N. benthamiana* leaf cells (Supplemental Fig. S6F). However, when we deleted the PrD from SSF, the localization appeared very different from intact SSF–GFP: SSFΔPrD was uniformly distributed in Arabidopsis cells and did not form fluorescent foci in *N. benthamiana* cells (Fig. 4B; Supplemental Fig. S6G).

To characterize SSF protein properties in vitro, we purified recombinant GFP–SSF with His tags at both termini (Supplemental Fig. S6H). Purified GFP–SSF formed liquid droplets upon the addition of the crowding agent polyethylene glycol (10% [w/v] PEG4000 (Boyko et al. 2019; Greig et al. 2020)). As a control, treating the same amount of purified GFP with PEG4000 did not yield similar results (Fig. 4C). Furthermore, a recombinant SSF protein lacking the PrD (GFP–SSFΔPrD) also did not show phase-separation even with 10% PEG treatment, suggesting that the PrD is required for the LLPS of SSF (Fig. 4C). SSF is an RBP, but it remains unknown whether SSF condensation can be influenced by RNA. To test this notion, we extracted total RNA from Col-0 and added it into the GFP–SSF solution. Importantly, the presence of RNA promoted GFP–SSF condensation even without PEG addition (Fig. 4D).

To explore the dynamics of GFP–SSF droplet formation, we added various concentrations of KCl to the recombinant GFP–SSF solution, which revealed that increasing KCl concentrations (250 to 1000 mM) or decreasing GFP–SSF protein concentrations disrupts the formation of GFP–SSF droplets, suggesting the reversibility of SSF phase separation (Fig. 4E; Supplemental Fig. S6I). Furthermore, we used a full laser beam to specifically bleach a portion of SSF–GFP or PrD(SSF)–GFP fluorescence and measured the recovery rate (Fang et al. 2019; Lu et al. 2020; Xie et al. 2020; Kim et al. 2021). We observed that the fluorescence of the bleached SSF–GFP region recovers to some extent (Supplemental Fig. S6, B and C), whereas PrD(SSF)–GFP fluorescence returned to the bleached area within 21 s (Fig. 4, F and G). Consistently, the droplets of recombinant GFP–SSF in solution recovered after photobleaching in vitro (Fig. 4, H and I), and showed a strong ability to fuse with each other, leading to the formation of progressively larger droplets (Fig. 4, J and K).

To further confirm that SSF can form droplets in vitro, we added 15% (w/v) Ficoll 400 to the GFP–SSF solution (Dao et al. 2018; Guo et al. 2019). We determined that GFP–SSF can form droplets after Ficoll addition, but GFP alone could not (Supplemental Fig. S6J). The formation of SSF droplets was not due to the added GFP tag, as recombinant mCherry–SSF exhibited a similar behavior (Fig. 4C; Supplemental Fig. S6K). Therefore, we propose that SSF undergoes LLPS, for which its PrD is essential.

## The SSF PrD contributes to the regulation of *FLC* transcription and flowering

As the formation of SSF droplets was affected by its PrD, we hypothesized that the function of SSF may be regulated by its PrD. To test this hypothesis, we used stable transgenic Arabidopsis lines harboring *proSSF:SSF* or *proSSF:SSFΔPrD* in the *ssf-2* background for phenotypic characterization. *ssf-2 proSSF:SSF* plants flowered later than *ssf-2*, while the *ssf-2 proSSF:SSFΔPrD* lines did not delay flowering to the same extent as the *proSSF:SSF* lines (Fig. 5, A and B), despite having comparable *SSF* transcript levels (Fig. 5C). To assess whether the PrD truncation affects SSF protein accumulation, we quantified the protein abundance of the GFP fusion in *ssf-2 proSSF:SSF–GFP* and *ssf-2 proSSF:SSFΔPrD–GFP* transgenic lines using an anti-GFP antibody: we observed no significant difference between the two transgenes (Supplemental Fig. S7). In agreement with the changes in flowering time, spliced and unspliced *FLC* transcript levels were higher in the *ssf-2 proSSF:SSF* lines than in *ssf-2*. However, *FLC* transcript levels were not higher in the *ssf-2 proSSF:SSFΔPrD* lines (Fig. 5, D and E), suggesting that the PrD is important for SSF to regulate *FLC* transcription.

We explored the function of the PrD of SSF by coinfiltrating *N. benthamiana* leaves with a reporter construct consisting of the *FLC* promoter driving the firefly LUC gene (*proFLC:LUC*) with either *35S:SSF* or *35S:SSFΔPrD* as effectors. The level of LUC activity indicated that removing the PrD inhibits the ability of SSF to promote *FLC* transcription (Fig. 5F). We further performed ChIP experiments to evaluate whether SSF might bind to *FLC* chromatin, and whether its PrD affects this binding, using *ssf-2 proSSF:SSF–GFP* and *ssf-2 proSSF:SSFΔPrD–GFP* transgenic plants. We determined that SSF–GFP can indeed bind to *FLC* chromatin, and the enrichment of SSFΔPrD–GFP on *FLC* was significantly reduced, with levels resembling Col-0 (Fig. 5G).

To further demonstrate that SSF requires PrD-triggered condensation to perform its molecular function, we replaced the SSF PrD with the low-complexity domain (LCD) of the RBP FUSCA (FUS), a domain important for protein LLPS (Lin et al. 2015; Patel et al. 2015). We generated *proSSF:SSF–PrDΔFUS* (encoding SSF–PrD with its PrD replaced with the FUS domain) and introduced this construct into *ssf-2*. The flowering time of these *ssf-2 proSSF:SSF–PrDΔFUS* lines was similar to that of *ssf-2 proSSF:SSF* lines, which was much later than that of *ssf-2* (Fig. 5H). Consistently, spliced and unspliced *FLC* transcript levels in *ssf-2 proSSF:SSF–PrDΔFUS* lines and *ssf-2 proSSF:SSF* lines were the same as Col-0, and their *SSF* expression levels were similar (Fig. 5, I to K). In agreement with these data, when we replaced the SSF PrD with the domain from FUS, LUC imaging showed that *35S:SSF–PrDΔFUS* promotes *FLC* transcription, similar to SSF in Col-0 (Fig. 5F). Moreover, we inspected GFP–SSF–PrDΔFUS characteristics in solution and observed that it can form liquid droplets, similar to GFP–SSF (Fig. 4C; Supplemental Fig. S6H). In addition, in transgenic Arabidopsis, we observed that

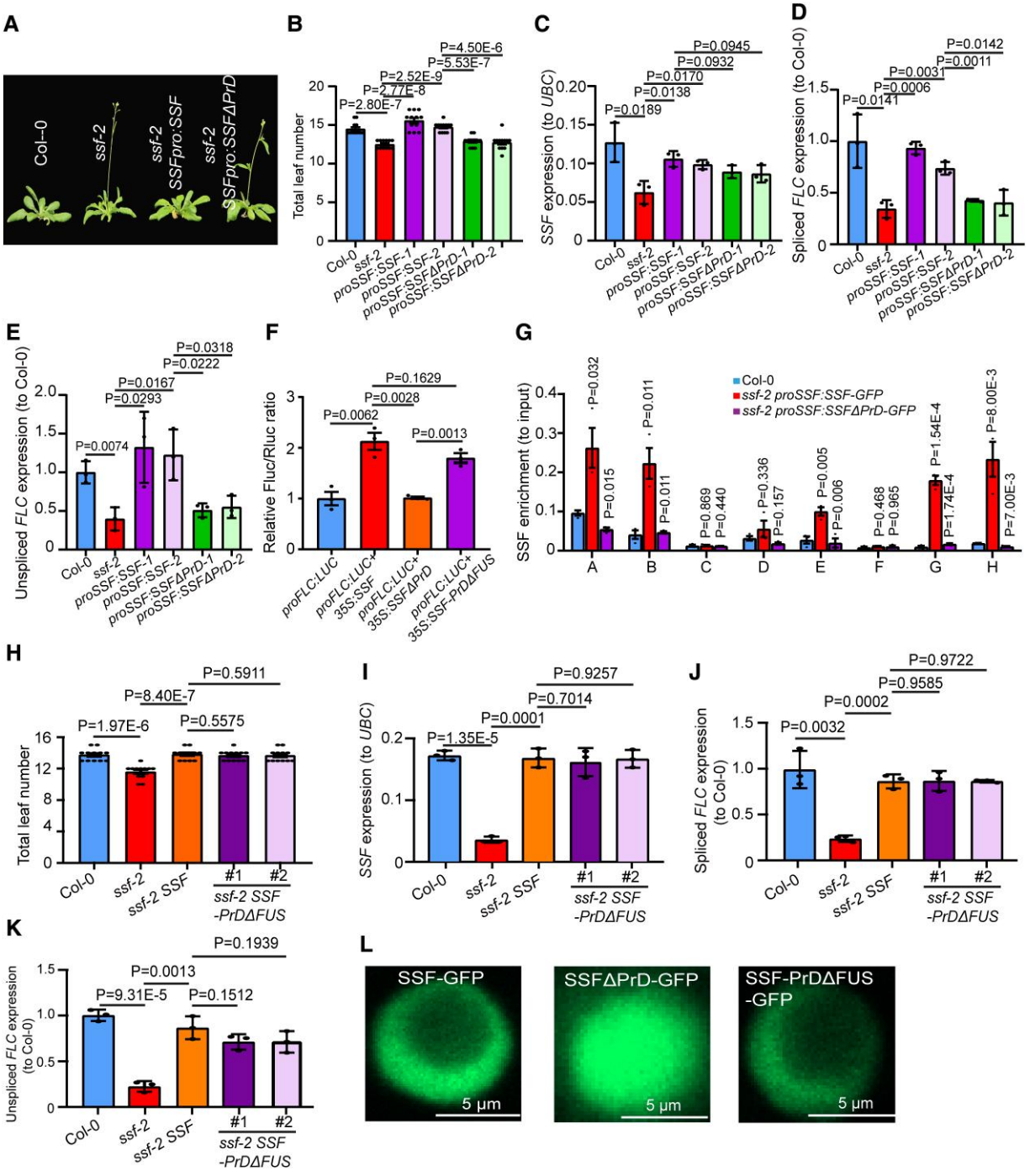


**Figure 5.** The prion-like domain of SSF is important for *FLC* transcription and flowering. **A)** Phenotype of Col-0, *ssf-2*, *ssf-2 proSSF:SSF* and *ssf-2 proSSF:SSFΔPrD*. **B)** PrD deletion affects the function of SSF in flowering time control. *proSSF:SSFΔPrD* failed to delay flowering time compared to the *proSSF:SSF* transgene. **C)** *SSF* transcript levels in Col-0, *ssf-2*, *ssf-2 proSSF:SSF* and *ssf-2 proSSF:SSFΔPrD*. **D** and **E)** Levels of spliced (**D**) and unspliced (**E**) *FLC* transcripts in Col-0, *ssf-2*, *ssf-2 proSSF:SSF* and *ssf-2 proSSF:SSFΔPrD* transgenic lines. **F)** PrD deletion (SSFΔPrD) and replacement with the FUS domain in SSF (SSF–PrDΔFUS) attenuates and enhances *FLCpro:LUC* expression, respectively. Firefly luciferase (Fluc) activity was normalized to *Renilla* luciferase (Rluc). **G)** SSF enrichment at *FLC* genomic regions is dependent on its PrD. The ChIP-qPCR primer positions are as indicated in the diagram in Fig. 2H. **H)** Flowering time analysis of Col-0, *ssf-2*, *ssf-2 proSSF:SSF* (*ssf-2 SSF*) and *ssf-2 proSSF:SSF–PrDΔFUS* (*ssf-2 SSF–PrDΔFUS*). **I)** *SSF* expression in Col-0, *ssf-2*, *ssf-2 SSF* and *ssf-2 SSF–PrDΔFUS*. **J** and **K)** Levels of spliced (**J**) and unspliced (**K**) *FLC* transcripts in Col-0, *ssf-2*, *ssf-2 SSF* and *ssf-2 SSF–PrDΔFUS*. **L)** Confocal micrographs showing the formation of nuclear bodies by SSF–GFP, SSFΔPrD–GFP and SSF–PrDΔFUS–GFP in transgenic Arabidopsis lines. Scale bars, 5 μm. In (**B** and **H**), data are means of 12 plants ± SEM. In (**C**–**E**, **I**–**K**), *UBC* was used as an internal control for qPCR, data are means of three independent experiments ± SD ($n = 50$ seedlings per replicate). In (**F**), data are means of three different leaves ± SEM. For each leaf, one area was infiltrated. In (**G**), data are means of three independent experiments ± SEM (3 g of seedlings per replicates). Significant differences were determined using Student's *t*-test. All experiments were performed at least 3 times, and representative results are shown.

SSF–PrDΔFUS displays a nonuniform distribution in the nucleus, similar to the distribution pattern of intact SSF (Fig. 5L). These data suggest that PrD-mediated condensation of SSF is important for its function in regulating *FLC* transcription and flowering time.

To explore whether the SSF PrD affects its interaction with DCP5, we carried out Y2H and LCI assays, which revealed that SSFΔPrD cannot interact with DCP5 (Fig. 1, A and B; Supplemental Fig. S1). We verified this finding by performing in vitro protein pull-down and Co-IP assays. Consistent with the LCI and Y2H assays, we did not detect interaction between SSFΔPrD and DCP5 in these experiments, suggesting that the PrD of SSF is required for its interaction with DCP5 (Supplemental Fig. S8, A and B). Interestingly, results of the Y2H, BiFC, and protein pull-down assays showed that SSF–PrDΔFUS still possesses the ability to interact with DCP5 (Supplemental Fig. S8, C to E).

## DCP5 exhibits phase separation in vivo

Detailed confocal imaging analysis of the *dcp5-1 proDCP5:DCP5–GFP* transgenic plants showed that DCP5–GFP accumulates in the cytosol and nuclear periphery, forming multiple speckles (Fig. 6A). PLAAC and D2P2 predicted highly disordered regions and two PrDs within DCP5 (Fig. 6B). To investigate whether DCP5 exhibits phase separation, we analyzed the fluidity of DCP5 in *proDCP5:DCP5–GFP* transgenic plants. Indeed, DCP5–GFP formed liquid droplets in the nucleus, whose fluorescence quickly recovered when a small region was photobleached with a full laser beam (Fang et al. 2019; Lu et al. 2020; Xie et al. 2020; Kim et al. 2021) (Fig. 6, C and D). Similarly, we observed that DCP5–GFP can form droplets in the nuclei of *N. benthamiana* leaf cells infiltrated with the *35S:DCP5–GFP* construct, and the fluorescence signal of the droplets recovered after photobleaching (Supplemental Fig. S9, A, C, and D). By contrast, deletion of the two PrDs from DCP5 resulted in a truncated protein unable to undergo LLPS in either transgenic Arabidopsis or *N. benthamiana* leaves (Fig. 6, C and E; Supplemental Fig. S9, B, C, and E). These results suggest that the DCP5 PrDs are essential for its LLPS.

## The PrD of DCP5 is important for regulating *FLC* transcription and flowering

To investigate whether DCP5 can trigger phase separation on its own in vitro, we purified recombinant mCherry–DCP5 from *Escherichia coli* (Supplemental Fig. S9F). Upon the addition of PEG or Ficoll (Dao et al. 2018; Boyko et al. 2019; Guo et al. 2019; Greig et al. 2020), recombinant mCherry–DCP5 underwent LLPS, but not mCherry. Moreover, without its PrDs, DCP5 lost the ability to undergo LLPS (Fig. 6F; Supplemental Fig. S9G). Even in vitro and without other cofactors, recombinant mCherry–DCP5 fluorescence recovered close to 90% of its original fluorescence signal following photobleaching (Fig. 6, G and H). The addition of KCl (0.25 to 1 M) to the protein solution reversed the phase separation of mCherry–DCP5 droplets (Fig. 6I; Supplemental Fig. S9H). Furthermore, small mCherry–DCP5 droplets could fuse to form larger ones (Fig. 6J).

To confirm the importance of PrDs in DCP5 function, we generated *35S:DCP5* and *35S:DCP5ΔPrD* constructs and transformed them into *dcp5-1*. The *dcp5-1 35S:DCP5* transgenic plants flowered earlier than *dcp5-1* (Fig. 7A). However, *dcp5-1 35S:DCP5ΔPrD* lines flowered significantly later than *dcp5-1 35S:DCP5* (Fig. 7A). Consistent with this result, *FLC* transcript levels in *35S:DCP5ΔPrD* lines were significantly higher than in *35S:DCP5* lines (Fig. 7, B and C), although their *DCP5* expression levels were comparable (Fig. 7D). Furthermore, when *proFLC:LUC* was coinfiltrated with *35S:DCP5* or *35S:DCP5ΔPrD* in *N. benthamiana*, DCP5 was able to downregulate *FLC* transcription, with the removal of the PrDs significantly decreasing the inhibitory effect of DCP5 on *FLC* transcription (Fig. 7, E and F). These results indicate that the PrDs of DCP5 are important for its LLPS and its ability to regulate *FLC* expression and flowering.

## DCP5 promotes the LLPS of SSF

We investigated the interaction between DCP5 and SSF with respect to LLPS by mixing equal amounts of purified recombinant GFP–SSF with His (control), DCP5 or DCP5ΔPrD. Notably, we observed that the addition of DCP5 significantly enlarges the droplet size of recombinant GFP–SSF compared to the addition of the His control, whereas DCP5ΔPrD showed no influence on GFP–SSF droplet size (Fig. 8, A and B). To better document this result, we performed semidenaturing detergent agarose gel electrophoresis (SDD-AGE) to evaluate the polymer size of prion-like protein using the method described for LLPS analysis (Ji et al. 2019). Indeed, the migration distance of GFP–SSF declined when DCP5 was added compared to His and DCP5ΔPrD. This result indicates that the addition of DCP5, but not the His tag or DCP5ΔPrD, increases GFP–SSF polymerization (Fig. 8C).

To obtain in vivo support for these results, we infiltrated *N. benthamiana* cells with constructs expressing *SSF–GFP* or *DCP5* from the 35S promoter. We observed stronger fluorescence from SSF–GFP droplets, as well as larger droplets, when coexpressed with *DCP5*, compared to coinfiltration of *SSF–GFP* with the empty vector (Fig. 8, D and E; Supplemental Fig. S10). We confirmed that the stronger fluorescence was not caused by a greater accumulation of SSF–GFP in these samples (Fig. 8F). We repeated these experiments with stable transgenic Arabidopsis lines expressing *SSF–GFP* and overexpressing *DCP5* and obtained similar results, showing that the plants harboring *SSF–GFP* and overexpressing *DCP5* have stronger fluorescence signals (Fig. 8, G and H) and formed larger SSF–GFP bodies than SSF–GFP without *DCP5* (Fig. 8I). In addition, *DCP5* transcript levels were not affected by loss of *SSF* function, and vice versa (Supplemental Fig. S11, A and B), and overexpression of *DCP5* did not affect SSF–GFP accumulation (Fig. 8J). These results suggest that DCP5 may promote SSF liquid condensation.

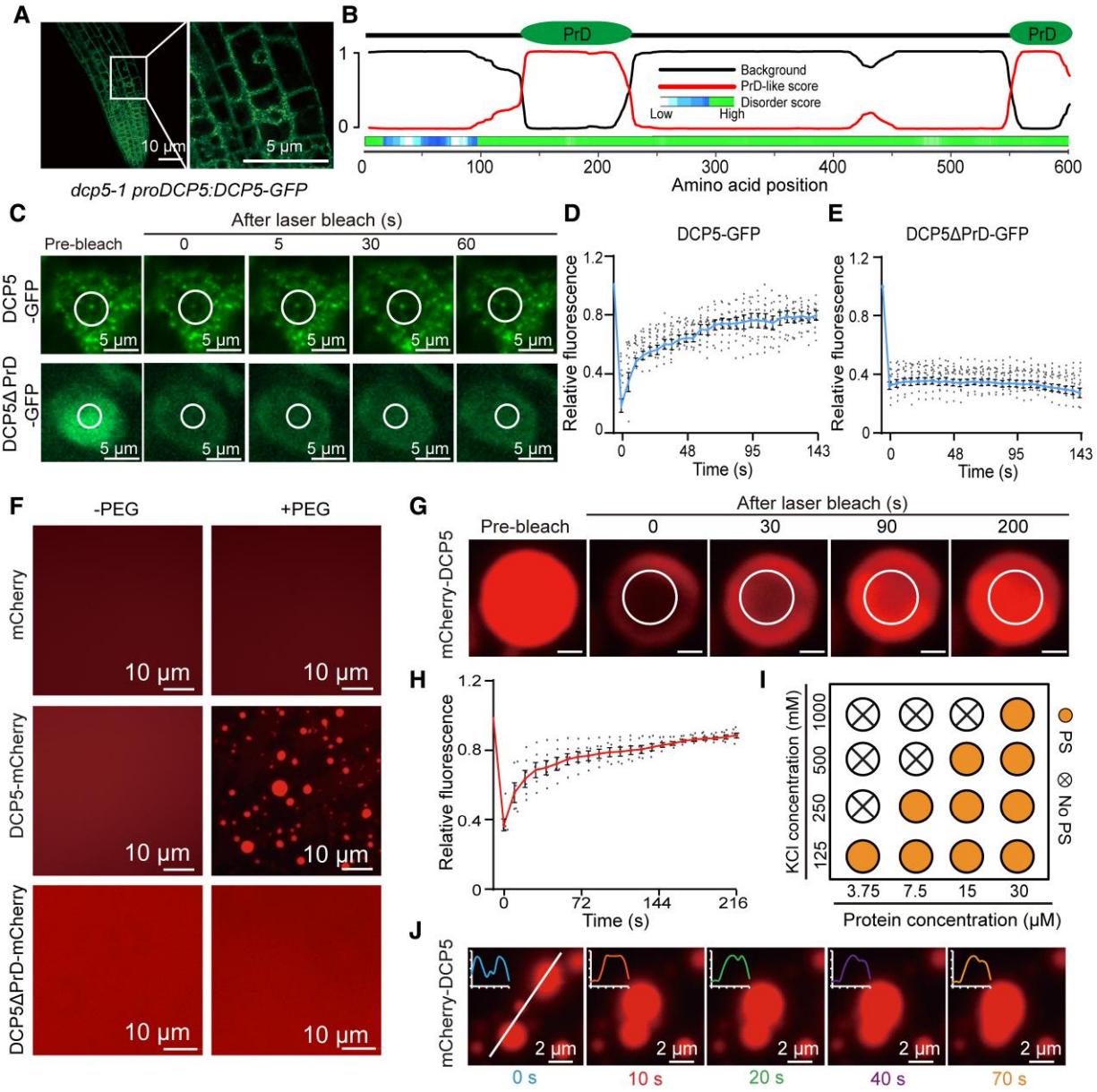


**Figure 6.** DCP5 exhibits liquid–liquid phase separation in vivo and in vitro. **A)** Fluorescence microscopy of root tips from 4-day-old transgenic seedlings expressing *DCP5–GFP*. Scale bars, 10 μm (left), 5 μm (right). **B)** Schematic diagram of DCP5 domains. Top, the position of two prion-like domains (PrDs); middle, PrD scores (0 to 1) predicted by the PLAAC algorithm; bottom, the score of disordered regions predicted by D2P2. **C)** Fluorescence time lapse microscopy of transgenic Arabidopsis expressing *DCP5–GFP* or *DCP5ΔPrD–GFP*. Scale bars, 5 μm. **D** and **E)** Quantification of fluorescence from the photobleached region ($n = 15$ nuclei). The images were taken every 3 s for 143 s to document fluorescence recovery, each time point was normalized to before photobleaching. **F)** Phase separation of mCherry–DCP5 upon PEG addition. mCherry alone was used as a control with the same amount of PEG. The design of mCherry–DCP5 is shown as Supplemental Fig. 9F; His tags were added to the two termini of DCP5 for protein purification. Scale bars, 10 μm. **G)** Fluorescence of mCherry–DCP5 recovered after photobleaching. Scale bars, 2 μm. **H)** Time course of fluorescence recovery after photobleaching of mCherry–DCP5 droplets ($n = 6$ droplets). The images were taken every 10 s over 216 s to document fluorescence recovery, each time point was normalized to before photobleaching. **I)** Illustration of DCP5 phase separation with different concentrations of mCherry–DCP5 protein and KCl. PS, phase separation. **J)** Merging of mCherry–DCP5 liquid droplets. At the upper left corner of each confocal micrograph, the fusion curve of mCherry–DCP5 is shown. Scale bars, 2 μm. In (**D**, **E**, and **H**), data are means of relative fluorescence ± SEM. Dots are relative fluorescence values. In (**C** and **G**), the circles indicate the photobleached regions. All experiments were performed at least 3 times, and representative results are shown.

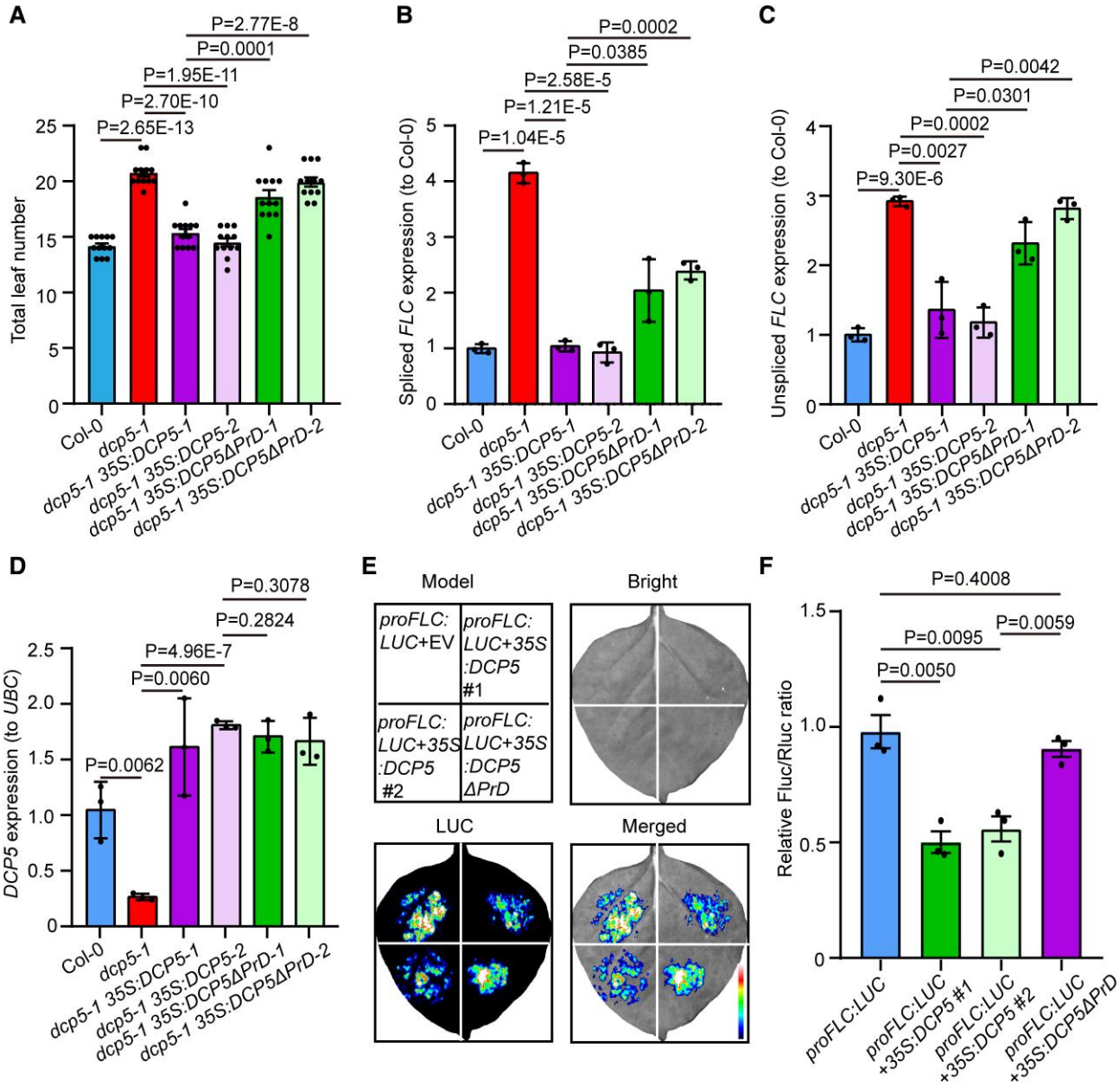


**Figure 7.** The prion-like domain (PrD) of DCP5 influences flowering time and *FLC* transcription. **A)** PrD deletion affects the function of DCP5 in flowering time control. *35S:DCP5ΔPrD* failed to promote flowering time compared to the *35S:DCP5* transgene. *DCP5ΔPrD*, *DCP5* with its *PrD* truncated. **B** to **D)** *FLC* and *DCP5* transcript levels in Col-0, *dcp5-1*, *dcp5-1 35S:DCP5* and *dcp5-1 35S:DCP5ΔPrD* transgenic lines. **E)** Overexpressing *DCP5ΔPrD* attenuates the inhibition of *proFLC:LUC* expression in *N. benthamiana*. For each leaf, one area was infiltrated. **F)** LUC activity derived from *proFLC:LUC* when coinfiltrated with *DCP5* or *DCP5ΔPrD*. LUC, luciferase; EV, empty vector. Firefly luciferase (Fluc) activity was normalized to *Renilla* luciferase (Rluc). In (**A**), data are means of 12 plants ± SEM. In (**B** to **D**), *UBC* was used as an internal control for qPCR, data are means of three independent experiments ± SD ($n = 50$ seedlings per replicate). In (**E**), for each leaf, one area was infiltrated. In (**F**), data are means of three independent leaves ± SEM. Significant differences were determined using Student's *t*-test. All experiments were performed at least 3 times, and representative results are shown.

In addition, when we mixed recombinant mCherry–DCP5 with SSF or His, we established that SSF has no clear influence on the size of DCP5 droplets (Supplemental Fig. S12, A and B), in contrast to the significant effect of DCP5 on SSF–GFP (Fig. 8, A and B). These results were supported by SDD-AGE assays showing that, similar to the addition of His alone, SSF cannot enhance the aggregation of mCherry–DCP5 (Supplemental Fig. S12C). Furthermore, when we crossed the *35S:DCP5–GFP* transgenic line into the *ssf-2* mutant, we observed no large difference in droplet size or number between *35S:DCP5–GFP* and *ssf-2 35S:DCP5–GFP* (Supplemental Fig. S12, D and E). We thus propose that SSF does not influence the LLPS of DCP5.

## The LLPS of DCP5–SSF contributes to *FLC* regulation

To determine the effect of DCP5 on the molecular function of SSF, we crossed *proSSF:SSF–GFP* with *DCP5*-OE and obtained

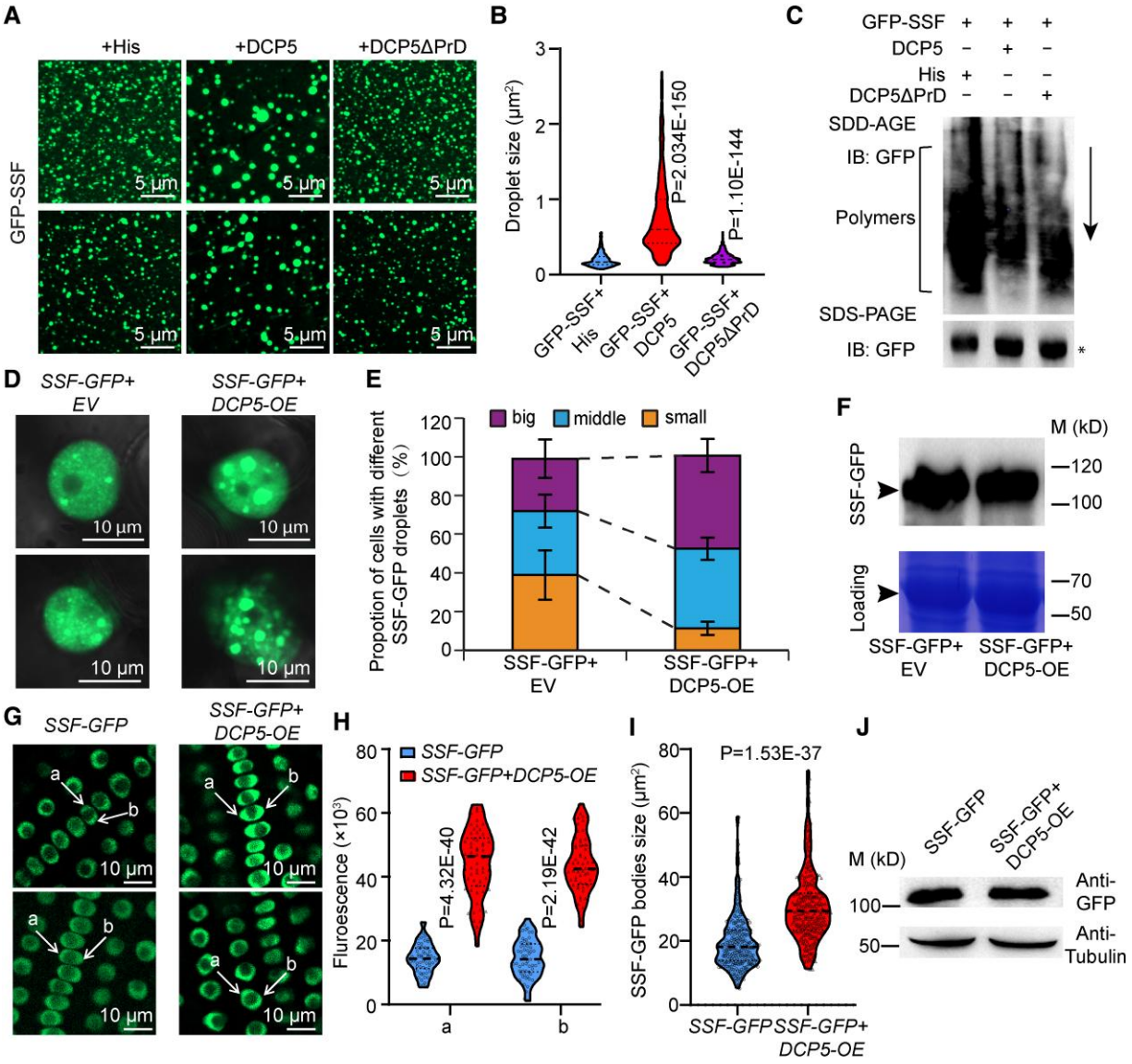


**Figure 8.** DCP5 promotes SSF liquid–liquid phase separation. **A)** DCP5, but not DCP5ΔPrD, can promote SSF liquid–liquid phase separation (LLPS) in solution. PrD, prion-like domain. His was used as a control, as DCP5 and DCP5ΔPrD were fused with His tags. *DCP5ΔPrD*, DCP5 with its PrD truncated. **B)** Quantification of GFP–SSF droplet size among the samples with the addition of the control protein (His), DCP5 or DCP5ΔPrD ($n = 934$). **C)** Semidenaturing detergent agarose gel electrophoresis (SDD-AGE) assays showing that GFP–SSF aggregates into larger polymers upon the addition of DCP5, compared to the addition of His or DCP5ΔPrD. The arrow indicates the direction of sample movement in the gel. **D)** DCP5 promotes the liquid separation of SSF–GFP in *N. benthamiana* cells. EV, empty vector. **E)** Quantification of droplet size between SSF–GFP and SSF–GFP with DCP5. Classification of droplet size: big: >3 μm$^2$; middle: 1 to 3 μm$^2$; small: <1 μm$^2$. EV, empty vector. Data are means ± SEM of 60 cells from multiple *N. benthamiana* leaves. **F)** The same amount of SSF–GFP protein was used for the assays in (**D** and **E**). **G** and **H)** Overexpression of *DCP5* promotes the liquid separation of SSF–GFP in Arabidopsis root cells ($n = 60$). The arrows in (**G**) indicate the representative unevenly distributed fluorescence signals. **I)** Overexpression of *DCP5* enlarges SSF–GFP droplet size ($n = 301$ root cells). **J)** *DCP5* overexpression does not influence SSF protein abundance. OE, overexpression. In (**B**, **H**, and **I**), significant differences were determined using Student's *t*-test. All experiments were performed at least 3 times, and representative results are shown.

transgenic plants harboring *proSSF:SSF–GFP* and *DCP5*-OE, which we used for ChIP analysis. We observed that DCP5 can promote SSF–GFP enrichment at the *FLC* locus (Fig. 9A). We sought to determine the molecular mechanism by which the DCP5–SSF complex modulates *FLC* expression. To this end, we transiently coinfiltrated *N. benthamiana* leaves with *proFLC:LUC* and *35S:DCP5ΔC* (Fig. 1G). Notably, DCP5ΔC failed to reduce *proFLC:LUC* expression compared to full-length DCP5, suggesting that the C-terminal region of DCP5 is important for *FLC* regulation. When we coinfiltrated *proFLC:LUC*, *35S:DCP5ΔC* and *35S:SSF* into *N. benthamiana* leaves, LUC activity increased (Fig. 9, B and C). By contrast, when *proFLC:LUC*,

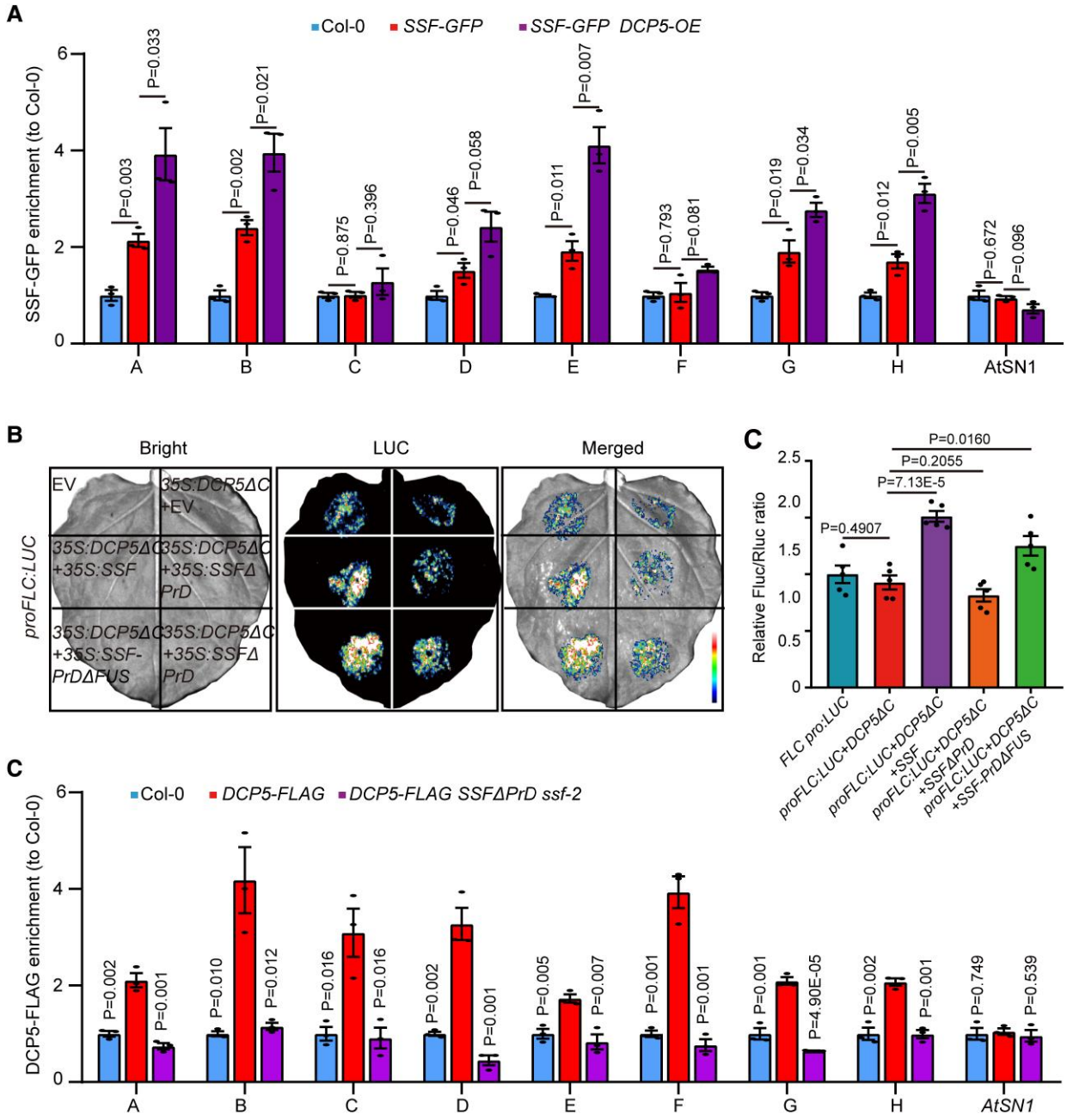


**Figure 9.** The liquid–liquid phase separation of SSF–DCP5 regulates flowering time. **A)** DCP5 enhances the enrichment of SSF to *FLC* genomic regions. **B** and **C)** *SSF* overexpression cannot promote the reduction of *proFLC:LUC* expression by DCP5ΔC in *N. benthamiana*. LUC, luciferase. EV, empty vector. In (**C**), firefly luciferase (Fluc) activity was normalized to *Renilla* luciferase (Rluc). **D)** DCP5–FLAG enrichment on *FLC* genomic regions is reduced in the presence of PrD-deleted SSF (*SSFΔPrD*). PrD, prion-like domain. The *P*-values illustrate significance level relative to *DCP5–FLAG*. *AtSN1*, negative control. In (**C**), data are means of LUC from five independent *N. benthamiana* leaves ± SEM. For each leaf, one area was infiltrated. In (**A** and **D**), the ChIP-qPCR primer positions are as indicated in the diagram in Fig. 2H, data are means three independent experiments ± SEM (3 g of seedlings per replicate). Significant differences were determined using Student's *t*-test. All experiments were performed at least 3 times, and representative results are shown.

*35S:DCP5ΔC* and *35S:SSFΔPrD* were coinfiltrated into *N. benthamiana* leaves, SSFΔPrD failed to promote LUC activity. Importantly, when *SSF–PrDΔFUS* was infiltrated instead of *SSFΔPrD*, LUC activity increased to a level similar to that seen with the coinfiltration of SSF (Fig. 9, B and C). These results suggest that SSF has an additional role in promoting *FLC* expression, which is independent from DCP5.

To confirm the relationship between *SSF* and *DCP5*, we transformed the *proSSF:SSFΔPrD* construct into *ssf-2 proDCP5:DCP5–FLAG* plants and generated *ssf-2 DCP5–*

*FLAG SSFΔPrD* transgenic plants, which were subjected to ChIP analysis using an anti-FLAG antibody. We determined that the enrichment of DCP5 at the *FLC* locus is significantly reduced in *ssf-2 DCP5–FLAG SSFΔPrD* compared to *DCP5–FLAG* plants (Fig. 9D). These results suggest that the regulation of *FLC* by the SSF–DCP5 complex requires the SSF PrD.

## Discussion

In this study, we show that DCP5 cooperates with SSF to regulate RNA Pol II enrichment, *FLC* transcription, and flowering time in Arabidopsis. Our genetic analysis of the *ssf-2 dcp5-1* double mutant and *ssf-2 DCP5*-OE transgenic lines suggests that DCP5 requires SSF to regulate *FLC* transcription and flowering (Fig. 3, A to J). In support of this claim, we discovered that DCP5 binds to the *FLC* genomic region in an SSF-dependent manner (Fig. 3K).

P-bodies have been previously proposed to be LLPS/biomolecular condensates (Banani et al. 2017). However, whether the phase separation of these components is the cause or the consequence of their molecular activity, such as gene silencing, is under debate (Eulalio et al. 2007). We provided several lines of evidence that DCP5 cellular condensates form by LLPS in vitro and in vivo (Fig. 6; Supplemental Fig. S9), and showed that the PrDs of DCP5 are necessary for its liquid phase separation (Fig. 6, C to G, Supplemental Fig. S9, C to E). However, although the PrD is required for DCP5 to form droplets (Fig. 6 and Supplemental Fig. S9), it is not necessary for interaction with SSF (Fig. 1, G and H). Through the analysis of transgenic Arabidopsis lines and transient expression assays, we discovered that variants of DCP5 lacking the PrD failed to repress *FLC* transcription and rescue the flowering time phenotype of the *dcp5-1* mutant (Fig. 7), suggesting that the LLPS of DCP5 is essential for its biological functions.

Mounting evidence indicates that LLPS of proteins can be complex, appearing in various forms varying from liquid-like, gel to solid (Patel et al. 2015; Noda et al. 2020). When observed under a confocal microscope, SSF–GFP did not show rounded foci (a property of LLPS [Patel et al. 2015]), but presented a nonuniform distribution in Arabidopsis cells (Fig. 4B). When using AX confocal techniques to observe Arabidopsis cells, we observed that SSF–GFP formed small puncta at these nonuniform regions (Supplemental Fig. S6A). Furthermore, in *N. benthamiana* cells and in vitro, SSF–GFP demonstrated the ability to reversibly form round droplets (Fig. 4, G to K; Supplemental Fig. S6, I to K). The recovery rate of SSF during fluorescence recovery after photobleaching was not strong (Supplemental Fig. S6, B and C). We speculate that SSF may be tightly assembled in vivo, similar to Tudor Staphylococcal Nuclease2, a component of stress particles in Arabidopsis (Gutierrez-Beltran et al. 2015), or some other stress granule components (Protter and Parker 2016); thus, SSF puncta are more solid. We replaced the PrD of SSF with the LCD of FUS, a domain important for LLPS in amyotrophic lateral sclerosis (ALS). By doing so, we determined that the resulting chimeric SSF–GFP showed a nonuniform distribution, rather than forming foci as found in ALS (Patel et al. 2015), suggesting that the SSF sequence outside of the PrD may have some influence on its LLPS. Importantly, variants of SSF without the PrD failed to rescue *FLC* transcript levels and the flowering time phenotype of the *ssf-2* mutant (Fig. 5, A to G). Notably, replacement of the SSF PrD with the FUS domain restored *FLC* expression to wild-type levels (Fig. 5, F and H–L), suggesting that SSF condensation is required for its regulation of *FLC* transcription.

The PrD of SSF is not only important for SSF droplet formation but also for interaction with DCP5 (Fig. 1, A to C and Supplemental Fig. S8, A and B). Therefore, it is difficult to determine whether the interaction is due to direct binding or a result of the LLPS of the two proteins. Interestingly, replacing the PrD of SSF with the FUS domain (SSF–PrDΔFUS) maintained the ability of SSF to interact with DCP5 (Supplemental Fig. S8, C to E). Different from interactions of well-folded domains, previous reports showed that specific motifs, so-called low-complexity aromatic-rich kinked segments (LARKS), can interact and assemble with proteins containing similar LARKS (Hughes et al. 2018; Mittag and Parker 2018). Both the FUS domain and SSF PrD contain such hydrophobic and aromatic amino acids, which provide the multivalent interactions for phase separation, although their sequences are very different (6.7% overall identity). These weak multivalent interactions in the FUS domain and SSF PrD may promote the interaction with DCP5, and it is possible that LLPS of these two proteins may facilitate their interaction. Further detailed site-specific mutagenesis analysis of the SSF PrD may help dissect these possibilities in future studies.

P-body components have been frequently reported to function mainly at the post-transcriptional level (Luo et al. 2018; Ivanov et al. 2019; Jang et al. 2019), although some do function in the nucleus. For instance, the LSM1–LSM7 complex is cytoplasmic and is involved in P-body formation and mRNA decay, whereas the LSM2–LSM8 complex is nuclear and plays a role in mRNA splicing (Perea-Resa et al. 2012). Here, we showed that DCP5 regulated *FLC* transcription; notably, ChIP assays indicated that RNA Pol II was highly enriched at the *FLC* locus in the *dcp5-1* mutant (Fig. 2G). In line with these data, the stability of *FLC* mRNA was comparable in *dcp5-1* and the wild-type Col-0 (Supplemental Fig. S4C). Therefore, we propose that DCP5 also functions in *FLC* regulation in the nucleus, but we cannot rule out its possible contribution at the post-transcriptional level, as it is also abundant in the cytosol (Fig. 2, E and F). Whether the other P-body components have functions in the nucleus similar to DCP5 warrants further study. For example, we also determined that DCP2, but not DCP1, interacted with SSF in the nucleus, and that *dcp2* mutants showed delayed flowering and higher *FLC* expression compared to wild-type Col-0 (Supplemental Fig. S13).

DCP5 was reported to be essential for the formation of P-bodies in Arabidopsis, as the *dcp5-1* knockdown mutant has smaller P-bodies of different shapes, although the

mechanism remains unclear (Xu and Chua 2009). Our data suggest that DCP5 promotes SSF LLPS (Fig. 8, Supplemental Fig. S10), but SSF does not promote that of DCP5 (Supplemental Fig. S12). The PrD of SSF is required for its binding to *FLC* chromatin (Fig. 5G), and more SSF–GFP was enriched at the *FLC* locus when *DCP5* was overexpressed (Fig. 9A). Therefore, DCP5-mediated SSF condensation may assist the SSF–DCP5 complex in binding to *FLC*. In line with this hypothesis, DCP5 function was SSF-dependent (Fig. 3). This conclusion was further supported by DCP5–FLAG ChIP assays; when overexpressing *SSFΔPrD*, the enrichment of DCP5 at the *FLC* loci was significantly reduced (Fig. 9D). Overall, these data suggest that LLPS is of significance for the SSF–DCP5 complex to regulate *FLC* transcription.

Hnisz et al. (2017) proposed a phase-separated multimolecular transcriptional model, which posits that phase separation plays a crucial role in transcriptional control. Accumulating evidence indicates that transcription involves the condensation of factors in the cell nucleus (Cramer 2019), and a phase-separation model involving RNA has been proposed for transcriptional control (Shao et al. 2022). Generally, dynamic phase-separated transcriptional condensates can assemble high concentrations of the transcriptional machinery complex to promote transcription initiation, thereby leading to proper transcriptional control (Sabari et al. 2018; Zhu et al. 2021). In this study, we discovered that SSF and DCP5 can phase separate and regulate RNA Pol II enrichment on *FLC* (Figs. 2G, 4 and 6), providing an additional layer of regulatory control for *FLC* transcription. Currently, it remains unclear how exactly the DCP5–SSF module affects RNA Pol II enrichment at *FLC*. Further efforts to determine whether the DCP5–SSF complex interacts with transcriptional machinery will be helpful.

We noticed that SSF promoted *FLC* transcription and delayed flowering, while DCP5 inhibited *FLC* transcription and promoted flowering (Fig. 3). Therefore, SSF and DCP5 show opposite effects on *FLC* transcription and flowering time regulation. This type of regulation involving the interaction between positive and negative factors has been reported in other studies. For example, MYC2 regulates the termination of jasmonate signaling through its interaction with MEDIATOR25 and MYC2-TARGETED BASIC HELIX-LOOP-HELIX TFs, which function differently to orchestrate jasmonate responses (Liu et al. 2019). We propose a model in which SSF may act as a "scaffold" protein anchored to the *FLC* locus that can interact with positive and negative regulatory factors to fine-tune *FLC* transcription. DCP5 represses *FLC* in an SSF-dependent manner (Fig. 3). Without a functional DCP5, such as DCP5ΔC, SSF presents a positive effect on *FLC* transcription (Fig. 9, B and C), suggesting that SSF may also associate with some activating factors (Fig. 10). Among the list of SSF-interacting proteins obtained from mass spectrometry analysis (Supplemental Data Set 1), we identified EARLY FLOWERING8 (ELF8; At2g06210), which is a homolog of a component of the Paf1 complex of budding yeast that promotes *FLC* expression (He et al. 2004). Whether the early flowering phenotype of SSF is ELF8-dependent requires further studies.

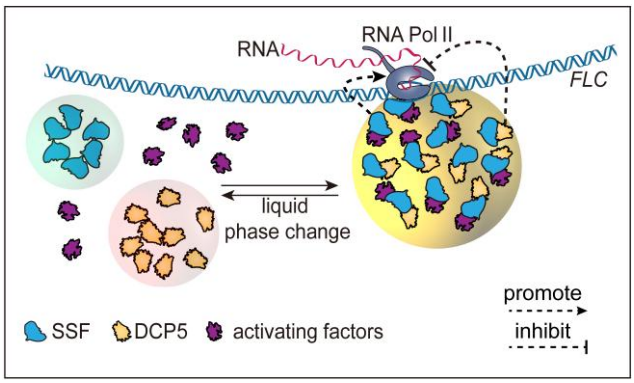


**Figure 10.** Proposed model for SSF and DCP5 in regulating *FLC* transcription. The dashed lines indicate multiple regulation steps.

In summary, this study reveals the role of the P-body component DCP5 in regulating *FLC* and flowering time. DCP5 interacts with SSF in the nucleus and regulates *FLC* transcription by affecting RNA Pol II enrichment in an LLPS-associated manner.

## Materials and methods

### Plant materials and growth conditions

The Col-0, *ssf-2* (SALK_028875), and *dcp5-1* (SALK_008881) Arabidopsis (*A. thaliana*) mutants were ordered from the Nottingham Arabidopsis Stock Centre (http://Arabidopsis.info). Seeds were surface sterilized with chlorine gas overnight, sown on Murashige and Skoog (MS) medium without sucrose, and stratified for 3 d at 5 °C in the dark before being transferred to long-day (16-h light/8-h dark, LED light [Philips, F25T8/TL841] intensity of 153 mmol $m^{-2}$ $s^{-1}$, 70% humidity) growth conditions at 22 °C for growth and phenotypic analysis, in addition to normal plant maintenance. The *N. benthamiana* plants were grown under the same growth conditions as Arabidopsis except that the temperature was set at 25 °C.

### Vector construction and transformation

For the *proDCP5:DCP5–GFP* and *proDCP5:DCP5–FLAG* constructs, the genomic sequence of *DCP5* encompassing a 1.6-kb promoter fragment, all exons, introns, and 1 kb of 3′ untranslated region was PCR-amplified from Col-0 genomic DNA using PrimerSTAR Max DNA polymerase (TakaraBio, Dalian, China, cat: R045Q). The *GFP* coding sequence (CDS) was amplified by PCR. In constructing *proDCP5:DCP5–FLAG*, the sequence encoding the FLAG tag was included in the reverse PCR primer for *DCP5* amplification. All DNA fragments were cloned using the pEASY-T3 Cloning vector (TransGen, Beijing, China, cat: CT301-01), and a single clone for each fragment was verified by Sanger sequencing and ligated into the pGreenII-0179 vector (Hellens et al. 2000) by

restriction enzyme digestion and ligation with T4 DNA ligase (TakaraBio, Dalian, China, cat: 2011A).

For *PrD(SSF)–GFP*, *SSFΔPrD–GFP* and *DCP5ΔPrD–GFP*, the CDSs of *SSF* and *DCP5* were amplified from first-strand cDNA prepared from total RNA of 2-week-old Col-0 seedlings, and the truncated *SSFΔPrD* and *DCP5ΔPrD* CDSs were amplified by overlapping PCR. All DNA fragments were sequenced and inserted into the pCAMBIA1305 vector (Novagen) downstream of the CaMV 35S promoter by restriction enzyme digestion and ligation, with the *GFP* CDS cloned in-frame and downstream of each target gene. Constructs harboring *mCherry* instead of *GFP* were generated following the same procedure. All constructs were transformed into Arabidopsis Columbia-0 (Col-0), *ssf-2*, or *dcp5-1* plants as described in the text by the floral dipping method (Clough and Bent 1998). The sequences of the primers used for vector construction are listed in Supplemental Table S1.

## Gene expression analysis

All gene expression analyses in this study were performed using 2-week-old seedlings grown under long-day conditions at 22 °C. Total RNA was extracted using Trizol reagent according to the manufacturer's instructions (Invitrogen, Waltham, MA, USA, cat: 15596-026). Reverse transcription was conducted using a one-step RNA reverse transcription kit (TakaraBio, Dalian, China, cat: RR086A) with gene-specific primers. Quantitative PCR was performed on a Roche LC480 LightCycler with gene-specific primers. Relative gene expression levels were normalized using *UBC* as a reference. The sequences of all primers are included in Supplemental Table S1. Three independent biological replicates were performed with approximately 50 seedlings per sample in each biological replicate. Data are shown as means ± SD of three replicate petri-dish plates with seedlings.

## Recombinant protein production and purification

The CDSs of the target genes were cloned into the pET28a (+) vector (EMD Biosciences, Novagen) and verified by sequencing. The resulting constructs were introduced into *E. coli* BL21 (DE3), selected in the presence of 50 μg/mL kanamycin, and confirmed by PCR. A single colony was inoculated into LB medium containing 50 μg/mL kanamycin and cultured at 37 °C until the $OD_{600}$ reached 0.6 to 0.8, after which 0.5 mM isopropyl β-D-1-thiogalactopyranoside (IPTG) was added to induce protein production overnight at 16 °C under constant shaking at 220 rpm. The bacterial cells were collected by centrifugation and sonicated, and the resulting mixture was centrifuged again. The supernatant was transferred to new tubes, mixed, and incubated with $Ni^{2+}$–NTA resin (Solarbio, Beijing, China, cat: P2010) at 4 °C for 2 h. An empty column was washed with wash buffer (50 mM $NaH_2PO_4$, 300 mM NaCl, 20 mM imidazole, pH 8.0), and then the $Ni^{2+}$–NTA slurry with the supernatant was loaded onto the column and allowed to settle by gravity. The resin was washed 3 times with wash buffer, and the target proteins were eluted with 250 mM imidazole. The purified protein was stored at 4 °C in stock solution (20 mM HEPES, pH 7.4, 150 mM KCl, 1 mM DTT). For long-term storage, the protein was stored at −80 °C.

## In vitro LLPS assay

Purified recombinant GFP fusion proteins kept in stock solution (20 mM HEPES, pH 7.4, 150 mM KCl, 1 mM DTT) were used for phase-separation tests. His–GFP–SSF–His, His–mCherry–SSF–His, His–GFP–SSFΔPrD–His, His–GFP–SSF–PrDΔFUS–His, His–mCherry–DCP5–His, and His–mCherry–DCP5ΔPrD–His were diluted to the indicated concentration and mixed gently with polyethylene glycol 4,000 (PEG4000, Sigma-Aldrich, Darmstadt, Germany, cat: 1.09727) or Ficoll (Ficoll 400, Solarbio, Beijing, China, cat: F8150), to a final PEG4000 and Ficoll 400 concentration of 10% and 15%, respectively (both w/v). After incubation at room temperature for 10 min, 5 to 10 μL of solution was transferred to glass slides and imaged by confocal microscopy (Zeiss LSM800, Jena, Germany; laser excitation: 488 nm, collection bandwidth: 500 to 530 nm, digital gain: 1.0). To check the influence of salt and protein concentration on phase separation, the same procedure was repeated, using different concentrations of KCl (250 to 1000 mM) followed by gentle mixing with the protein solution before microscopy examination. To check the influence of RNA on LLPS, the above procedure was performed, with total RNA extracted from Col-0 gently mixed with 12.8 μM GFP–SSF protein solution to a final concentration of 0.6 μg/μL (Fang et al. 2019; Zhang et al. 2019), but no PEG4000 treatment was applied.

## Photobleaching and fluorescence recovery assays

For in vivo tests, the roots of transgenic Arabidopsis seedlings expressing *SSF–GFP* or *DCP5–GFP* were used for fluorescence imaging with a confocal microscope. After the target regions were focused and imaged, a small portion of GFP signal was bleached with 10 iterations at 100% intensity of the laser beam (Zeiss LSM800, Jena, Germany; laser excitation: 488 nm, collection bandwidth: 500 to 530 nm, digital gain: 1.0). For photobleaching of mCherry, 20 iterations at 100% intensity of laser beam (Zeiss LSM800, Jena, Germany; laser excitation: 561 nm, collection bandwidth: 560 to 650 nm, digital gain: 1.0) were used. For the tests in *N. benthamiana*, 20 iterations at 100% intensity of the laser beam at 488 nm were applied. The fluorescence of each image was collected and quantified using the Zeiss confocal imaging system to generate a recovery curve. After reading the fluorescence data with a Zeiss 800 confocal microscope, we used the values before photobleaching as benchmark and compared the values at each time point to generate a relative fluorescence curve. For super resolution imaging of SSF condensates in cells, the roots of transgenic Arabidopsis seedlings expressing *SSF–GFP* were captured by AX with NSPARC (Nikon Spatial Array Confocal; a confocal-based super resolution microscope).

For in vitro tests, purified recombinant GFP fusion proteins were mounted onto glass slides and visualized by confocal microscopy as above, but fluorescence bleaching was

performed using 50 iterations at 100% intensity of the laser beam at 488 nm.

## Dual-LUC assay

The 1.6-kb *FLC* promoter was cloned into the pGreenII 0800-LUC vector to generate *proFLC:LUC* (Wang et al. 2020). *DCP5*, *DCP5ΔPrD*, *SSF*, *SSFΔPrD*, and *SSF–PrDΔFUS* overexpression constructs (pGreenII 0800-miRNA and pGreenII-0800-LUC, driven by the 35S promoter; Miaolingbio, China) were obtained by restriction enzyme cloning. Different vectors were individually transformed into Agrobacterium (*Agrobacterium tumefaciens*) strain GV3101 cells and the appropriate combinations were infiltrated into *N. benthamiana* leaves. After 3 days of growth, LUC activity was captured and analyzed with a Tanon 5,200 chemiluminescent imaging system (Tanon, Shanghai, China). A Dualucif™ Firefly & Renilla Assay kit (BioScience, Shanghai, China, cat: F6075M) was used for the quantitative analysis of LUC activity. Total plant protein was extracted and used to measure the LUC activity of Fluc (Firefly LUC) and Rluc (*Renilla* LUC) with a TriStar² LB 942-multimode microplate reader. The Fluc data were normalized to Rluc to represent the relative *proFLC:LUC* activity in different samples. Three replicates from different *N. benthamiana* leaves that had been injected were performed for each analysis. Data are shown as means ± SEM of three independent replicate *N. benthamiana* leaves.

## Yeast two-hybrid assay (Y2H)

The CDSs of *SSF*, *SSFΔPrD*, *SSF$^{WW}$*, *SSF–PrDΔFUS*, and *FCA* were cloned in-frame with the sequence encoding the GAL4 DNA-binding domain in the bait vector pGBKT7, while the CDSs of *DCP5* and *SSF* were cloned in-frame with the sequence encoding the GAL4 activation domain in the prey vector pGADT7 (CLONTECH). Pairs of constructs were co-transformed into yeast (*S. cerevisiae*) strain AH109 and selected on synthetic defined (SD) medium lacking tryptophan and leucine for 3 d (SD–WL). Colonies were then resuspended and washed 3 times in SD medium lacking tryptophan, leucine, histidine, and adenine (SD–WLHA) and plated onto the same selection medium. After 3 to 4 d, yeast growth was checked and photographs were taken. As positive controls, the pGBK-p53 and pGAD-T constructs were used; negative controls were provided by transforming each target vector with empty pGBKT7 or pGADT7 according to the manufacturer's instructions.

## Luciferase complementation imaging (LCI) and bimolecular fluorescence complementation (BiFC) assays

LCI assays were conducted in *N. benthamiana* leaves as described (Chen et al. 2008). The CDSs of *SSF* and *DCP5* were cloned in-frame with the sequence encoding the N- or C-terminal halves of LUC, respectively. All constructs were then individually introduced into Agrobacterium strain GV3101. The bacteria were grown in LB overnight, collected by centrifugation and resuspended to an OD600 of 1.0 in infiltration buffer (0.01 M MES, 0.01 mM $MgCl_2$, 0.1 mM acetosyringone), and coinfiltrated as appropriate pairs into *N. benthamiana* leaves. Three days later, D-luciferin (5 mg/mL) was sprayed onto the leaves and luminescence was monitored with a Tanon 5,200 chemiluminescent imaging system (Tanon, Shanghai, China). The constructs *nLUC-SSF$^{ww}$* and *DCP5-cLUC*, or *nLUC-SSFΔPrD* and *DCP5-cLUC*, were coinfiltrated as negative controls. BiFC assays were performed in Arabidopsis protoplasts (Wang et al. 2020). The *SSF* CDS was cloned in-frame with the sequence encoding the N-terminal half of YFP (pUC-SPYNE), while the *DCP5* CDS was cloned in-frame with the sequence encoding the C-terminal half of YFP (pUC-SPYCE). The resulting constructs were transfected into Arabidopsis protoplasts via PEG-mediated transfection as previously described (Yoo et al. 2007). After incubation in the dark overnight, protoplasts were imaged for YFP fluorescence analysis with a Zeiss confocal microscope (Zeiss LSM800, Jena, Germany; laser excitation: 488 nm, collection bandwidth: 500 to 530 nm, digital gain: 1.0).

## Pull-down assays

For protein pull-down assays, constructs encoding GFP–SSF, GFP–SSFΔPrD, GFP–SSF–PrDΔFUS, mCherry–DCP5, and GFP were generated and introduced into *E. coli* BL21 (DE3). Protein production was induced by the addition of IPTG (final concentration: 0.5 mM) to bacterial cultures grown at 16 °C. The cells were collected by a brief centrifugation, sonicated (15 s on/90 s off for 16 times) and centrifuged again to collect cell debris. The supernatants containing different recombinant proteins were mixed and incubated at 4 °C for 4 h. GFP Trap beads (ChromoTek, Chicago, Illinois, USA, cat: gtm-20) were prepared and incubated with the supernatant mixture at 4 °C for at least 4 h and then washed with 20 mM Tris–HCl, pH 7.5. Finally, the beads were collected by centrifugation, resuspended in protein loading buffer, boiled, and centrifuged again. Eluted proteins were separated by SDS-PAGE for immunoblot analysis with an anti-mCherry antibody (EnoGene, Nanjing, Jiangsu, China, cat: E12-010, dilution: 1/2,000).

## Co-IP analysis

For in vivo Co-IP assays, the *proSSF:SSF–GFP* transgenic line was crossed to the *proDCP5:DCP5–FLAG* transgenic line to obtain the *SSF–GFP DCP5–FLAG* line. F3 generation seeds were sown on MS medium and seedlings were collected after 2 weeks of growth at 22 °C under long-day conditions. Total proteins were extracted from whole Arabidopsis seedlings at 4 °C in extraction buffer (50 mM Tris–HCl pH 8.0, 150 mM NaCl, 0.1% [v/v] IGEPAL, 2.5 mM EDTA pH 8.0, 10% [v/v] glycerol, 10 mM β-mercaptoethanol, 1 mM PMSF, 10 μM leupeptin, and 1×Roche protease inhibitor cocktail [Roche, Basel, Swiss]). The extracts were centrifuged at 13,523 × *g* at 4 °C for 10 min several times until the supernatant was clear. Trap beads were prepared, added to the protein extracts and incubated at 4 °C for at least 4 h. After three washes with TBT buffer

(0.02 M Tris–HCl pH8.0, 150 mM NaCl, 0.1% [v/v] Triton X-100, 0.1% [v/v] Tween 20), the beads were boiled in SDS loading buffer and separated by SDS-PAGE for immunoblot analysis. The target proteins were detected with anti-GFP (Roche, Basel, Swiss, cat: 11414460001, dilution: 1/1,000) or anti-FLAG (MBL, Sapporo, Hokkaido, Japan, M185, dilution: 1/10,000) antibodies.

## Nucleo-cytoplasmic separation and immunoblot analysis

Cytoplasmic and nuclear proteins were sequentially isolated from 1 g of *proDCP5:DCP5–FLAG* transgenic seedlings using a sucrose gradient protocol as previously described (Zavaliev et al. 2020). Two-week-old Arabidopsis seedlings were ground to a fine powder in liquid nitrogen. The powder was resuspended in lysis buffer (20 mM Tris–HCl, pH 7.5, 20 mM KCl, 2 mM EDTA, 2.5 mM $MgCl_2$, 25% [v/v] glycerol, 0.25 M sucrose, 5 mM DTT, 1 mM PMSF, 1×protein inhibitor cocktail) and incubated at 4 °C for 10 min. The samples were filtered through Miracloth (Millipore, Darmstadt, Germany, cat: 475855-1R) to remove cell debris, and the cleared supernatant was centrifuged at 1,500 × *g* at 4 °C for 20 min. The supernatant was collected as the cytosolic extract. The remaining supernatant was collected again by centrifugation at 10,000 × *g* at 4 °C for 15 min and transferred to the cytosolic extract tube. The pellet was washed 4 times with 5 mL of NRBT buffer (20 mM Tris–HCl, pH 7.4, 25% [v/v] glycerol, 2.5 mM $MgCl_2$, and 0.2% [v/v] Triton X-100). After the last wash, the pellet was resuspended with 500 µL of NRB2 buffer (20 mM Tris–HCl, pH 7.5, 0.25 M sucrose, 10 mM $MgCl_2$, 0.5% [v/v] Triton X-100, 1×protein inhibitor cocktail and 5 mM β-mercaptoethanol). The resulting suspension was layered at 1:1 on top of NRB3 buffer (20 mM Tris–HCl, pH 7.5, 1.7 M sucrose, 10 mM $MgCl_2$, 0.5% [v/v] Triton X-100, 1×protein inhibitor cocktail and 5 mM β-mercaptoethanol) and centrifuged at 16,000 × *g* for 1 h at 4 °C. The top layer was removed and the pellet was resuspended with 600 µL of plant extraction buffer containing 1% (v/v) Triton X-100, 1×protease inhibitor cocktail and 5 mM β-mercaptoethanol to collect the nuclear fraction. The nuclear and cytoplasmic fractions were then separated by SDS-PAGE for immunoblot analysis with anti-FLAG (MBL, Sapporo, Hokkaido, Japan, cat: M185, dilution: 1/10,000), anti-Actin (EnoGene, Nanjing, Jiangsu, China, cat: E20-53034, dilution: 1/3,000), or anti-Histone H3 antibodies (Abcam, Cambridge, UK, cat: ab1791, dilution: 1/2,000).

## mRNA decay analysis

mRNA decay analysis was performed as previously described (Tong et al. 2022). Briefly, 14-day-old Col-0, *dcp5-1* and *ssf-2* seedlings were incubated in 3 mL of incubation buffer (1 mM Tris–HCl pH 7.5, 1 mM NaCl, 1 mM KCl, 15 mM sucrose) with rotation at 75 rpm in 12-well plates for 15 min. The incubation solution was then replaced with 3 mL of fresh buffer containing 1 mM cordycepin (Solarbio, Beijing, China, cat: 70-03-0). Samples incubated at 22 °C were harvested at different time points (0.5, 1, 2, 4, 6, and 12 h), frozen in liquid nitrogen, and subjected to total RNA isolation and RT-qPCR analysis as described above. Each RT-qPCR was performed independently for three biological replicates with approximately 50 seedlings per sample in each biological replicate. Data are shown as means ± SEM of three replicate plates with seedlings.

## SDD-AGE assay

The assay was performed as described by Ji et al. (2019). Briefly, after production and purification of recombinant proteins in *E. coli* (DE3), loading buffer (0.5× Tris borate EDTA [TBE] pH 8.0, 10% [v/v] glycerol, 2% [w/v] SDS, 0.0025% [w/v] bromophenol blue) was added to the protein solution and incubated at room temperature for 15 min. A freshly prepared 1.5% (w/v) agarose gel in 1× TBE containing 0.1% (w/v) SDS was prerun in running buffer (1× TBE containing 0.1% [w/v] SDS) at 4 °C with an electrophoresis voltage of 100 V for 1 h, before loading and separating the protein samples under the same conditions for 1 h. Finally, the separated proteins were transferred to a PVDF membrane (Millipore, Darmstadt, Germany) for immunoblot analysis using anti-GFP (Roche, Basel, Swiss, cat: 11414460001, dilution: 1/1,000), or anti-mCherry (EnoGene, Nanjing, Jiangsu, China, cat: E12-010, dilution: 1/2,000) antibodies. This method was used to detect proteins containing prion-like domains. The ability of the protein to form droplets is judged by its migration distance in the gel. The longer the migration distance, the weaker the ability to form droplets, and vice versa.

## ChIP assays

ChIP assays for RNA Pol II, SSF–GFP and DCP5–GFP at the *FLC* locus were conducted as detailed in the previous publications (Li et al. 2015; Wang et al. 2020). First, 3 g of seedlings grown under long-day conditions for 2 weeks were crosslinked with 1% (w/v) formaldehyde, and the nuclei were extracted in Honda Buffer (0.44 M sucrose, 1.25% [w/v] Ficoll, 2.5% [w/v] Dextran T40, 20 mM HEPES KOH pH 7.4, 0.5% [v/v] Triton X-100, 10 mM $MgCl_2$, 5 mM DTT, protease inhibitor cocktail [cOmplete, Roche, Basel, Swiss]) and sonicated. After chromatin was prewashed with protein A/G magnetic beads, the protein–DNA complex was precipitated with anti-GFP (Abcam, Cambridge, UK, cat: ab290), anti-FLAG (SIGMA, Darmstadt, Germany, SAB4301135), or anti-Pol II (Abcam, Cambridge, UK, 8WG16 cat: ab817) antibodies. The protein–DNA complex was reverse crosslinked overnight with 0.2 M NaCl at 65 °C. DNA was extracted, purified, and amplified by qPCR. For the Pol II ChIP, Col-0, *dcp5-1*, and *dcp5-1 proDCP5:DCP5–GFP* transgenic plants were used. For the SSF–GFP ChIP, Col-0, *ssf-2 proSSF:SSF–GFP*, *DCP5*-OE *proSSF:SSF–GFP*, and *ssf-2 proSSF:SSFΔPrD–GFP* plants were used. For the DCP5–GFP ChIP, Col-0 and *dcp5-1 proDCP5:DCP5–GFP* transgenic plants, as well as *ssf-2 proDCP5:DCP5–GFP* plants, were used. For the DCP5–FLAG ChIP, Col-0 and *dcp5-1 proDCP5:DCP5–FLAG* transgenic plants, as well as *proSSF:SSFΔPrD proDCP5:DCP5–GFP* plants were used. *P5SC1-II* was used as the positive control (Zhang et al. 2022). Gene-specific ChIP primers are shown in

Supplemental Table S1. Each qPCR was performed independently for three biological replicates. Three independent biological replicates from different plates of Arabidopsis seedlings were performed with approximately 3 g of seedlings per sample in each biological replicate. Data are shown as means ± SEM of three replicate plates.

### Statistical analysis

All statistical tests analyses were conducted in GraphPad Prism version 8 (GraphPad Software, http://www.graphpad.com) and SPSS. A two-tailed Student's *t*-test was performed. The detailed statistical results are shown in Supplemental Data Set 2.

### Accession numbers

Accession numbers based on The Arabidopsis Information Resource (https://www.arabidopsis.org) for all genes examined in this study are *SSF* (AT2G47310), *DCP5* (AT1G26110), *FCA* (AT4G16280), *DCP1* (AT1G08370), *DCP2* (AT5G13570), and *UBC* (At1g50490).

## Acknowledgments

We thank Dr Shujia Li from Yonghong Wang's lab (Institute of Genetics and Developmental Biology, Chinese Academy of Sciences) for help with the generation of *DCP5–GFP* transgenic *Arabidopsis thaliana* plants, and the members of the Li lab for value discussion.

## Author contributions

P.L., W.W., C.W., and Y.W. designed the experiments and analyzed the data. W.W., C.W., Y.W., J.M., T.W., Z.T., P.L., S.L., Y.H., A.G., H.W., and C.Q. performed the experiments. P.L. and W.W. wrote the manuscript.

## Supplemental data

The following materials are available in the online version of this article.

**Supplemental Figure S1**. Additional data of the interaction between SSF and DCP5 (supports Fig. 1).

**Supplemental Figure S2**. FCA does not interact with DCP5 or SSF (supports Fig. 1).

**Supplemental Figure S3**. Localization of different DCP5 truncations in *Nicotiana benthamiana* cells (supports Fig. 1).

**Supplemental Figure S4**. Identification of the *dcp5-1* mutant and *FLC* mRNA stability analysis in *dcp5-1* and *ssf-2* (supports Fig. 2).

**Supplemental Figure S5**. Phenotype of transgenic plants overexpressing *DCP5* in wild-type Col-0 and in the *ssf-2* mutant background (supports Fig. 3).

**Supplemental Figure S6**. Additional data for SSF phase separation in vivo and in vitro (supports Fig. 4).

**Supplemental Figure S7**. The PrD does not affect SSF abundance (supports Fig. 5).

**Supplemental Figure S8**. The PrD of SSF is important for its interaction with DCP5 (supports Fig. 5).

**Supplemental Figure S9**. Additional supporting data for DCP5 LLPS in vivo and in vitro (supports Fig. 6).

**Supplemental Figure S10**. DCP5 promotes the LLPS of SSF–GFP (supports Fig. 8).

**Supplemental Figure S11**. DCP5 and SSF do not reciprocally influence the transcript levels of their encoding genes (supports Fig. 8).

**Supplemental Figure S12**. SSF does not promote DCP5 LLPS (supports Fig. 8).

**Supplemental Figure S13**. DCP2, but not DCP1, interacts with SSF and *DCP2*-RNAi plants are late flowering (supports Fig. 2).

**Supplemental Table S1**. Primers used in this study.

**Supplemental Data Set 1**. Components of the SSF complex analyzed in this study.

**Supplemental Data Set 2**. Statistical analyses.

## Funding

This work was supported by the National Key Research and Development Program of China (2022YFD1201803), the Anhui Provincial Major Science and Technology Project (202203a06020005), the National Natural Science Foundation of China (32171954), and the Anhui Provincial Natural Science Foundation (2008085QC121).

*Conflict of interest statement.* None declared.

## References

**Banani SF, Lee HO, Hyman AA, Rosen MK**. Biomolecular condensates: organizers of cellular biochemistry. Nat Rev Mol Cell Biol. 2017:**18**(5):285–298. https://doi.org/10.1038/nrm.2017.7

**Boija A, Klein IA, Sabari BR, Dall'Agnese A, Coffey EL, Zamudio AV, Li CH, Shrinivas K, Manteiga JC, Hannett NM, et al.** Transcription factors activate genes through the phase-separation capacity of their activation domains. Cell. 2018:**175**(7):1842–1855.e1816. https://doi.org/10.1016/j.cell.2018.10.042

**Boyko S, Qi X, Chen TH, Surewicz K, Surewicz WK**. Liquid-liquid phase separation of tau protein: the crucial role of electrostatic interactions. J Biol Chem. 2019:**294**(29):11054–11059. https://doi.org/10.1074/jbc.AC119.009198

**Chen H, Zou Y, Shang Y, Lin H, Wang Y, Cai R, Tang X, Zhou JM**. Firefly luciferase complementation imaging assay for protein-protein interactions in plants. Plant Physiol. 2008:**146**(2):368–376. https://doi.org/10.1104/pp.107.111740

**Clough SJ, Bent AF**. Floral dip: a simplified method for Agrobacterium-mediated transformation of *Arabidopsis thaliana*. Plant J. 1998:**16**(6):735–743. https://doi.org/10.1046/j.1365-313x.1998.00343.x

**Collier S, Pendle A, Boudonck K, van Rij T, Dolan L, Shaw P**. A distant coilin homologue is required for the formation of cajal bodies in Arabidopsis. Mol Biol Cell. 2006:**17**(7):2942–2951. https://doi.org/10.1091/mbc.e05-12-1157

**Cramer P**. Organization and regulation of gene transcription. Nature. 2019:**573**(7772):45–54. https://doi.org/10.1038/s41586-019-1517-4

**Crevillen P, Dean C**. Regulation of the floral repressor gene *FLC*: the complexity of transcription in a chromatin context. Curr Opin Plant Biol. 2011:**14**(1):38–44. https://doi.org/10.1016/j.pbi.2010.08.015

**Dao TP, Kolaitis RM, Kim HJ, O'Donovan K, Martyniak B, Colicino E, Hehnly H, Taylor JP, Castaneda CA**. Ubiquitin modulates liquid-liquid phase separation of UBQLN2 via disruption of multivalent interactions. Mol Cell. 2018:**69**(6):965–978.e966. https://doi.org/10.1016/j.molcel.2018.02.004

**Emenecker RJ, Holehouse AS, Strader LC**. Emerging roles for phase separation in plants. Dev Cell. 2020:**55**(1):69–83. https://doi.org/10.1016/j.devcel.2020.09.010

**Eulalio A, Behm-Ansmant I, Schweizer D, Izaurralde E**. P-body formation is a consequence, not the cause, of RNA-mediated gene silencing. Mol Cell Biol. 2007:**27**(11):3970–3981. https://doi.org/10.1128/MCB.00128-07

**Fang X, Wang L, Ishikawa R, Li Y, Fiedler M, Liu F, Calder G, Rowan B, Weigel D, Li P, et al.** Arabidopsis FLL2 promotes liquid-liquid phase separation of polyadenylation complexes. Nature. 2019:**569**(7755):265–269. https://doi.org/10.1038/s41586-019-1165-8

**Greig JA, Nguyen TA, Lee M, Holehouse AS, Posey AE, Pappu RV, Jedd G**. Arginine-enriched mixed-charge domains provide cohesion for nuclear speckle condensation. Mol Cell. 2020:**77**(6):1237–1250.e1234. https://doi.org/10.1016/j.molcel.2020.01.025

**Guo YE, Manteiga JC, Henninger JE, Sabari BR, Dall'Agnese A, Hannett NM, Spille JH, Afeyan LK, Zamudio AV, Shrinivas K, et al.** Pol II phosphorylation regulates a switch between transcriptional and splicing condensates. Nature. 2019:**572**(7770):543–548. https://doi.org/10.1038/s41586-019-1464-0

**Gutierrez-Beltran E, Moschou PN, Smertenko AP, Bozhkov PV**. Tudor staphylococcal nuclease links formation of stress granules and processing bodies with mRNA catabolism in Arabidopsis. Plant Cell. 2015:**27**(3):926–943. https://doi.org/10.1105/tpc.114.134494

**He Y, Doyle MR, Amasino RM**. PAF1-complex-mediated Histone methylation *of FLOWERING LOCUS C* chromatin is required for the vernalization-responsive, winter-annual habit in Arabidopsis. Genes Dev. 2004:**18**(22):2774–2784. https://doi.org/10.1101/gad.1244504

**Hellens RP, Edwards EA, Leyland NR, Bean S, Mullineaux PM**. Pgreen: a versatile and flexible binary Ti vector for Agrobacterium-mediated plant transformation. Plant Mol Biol. 2000:**42**(6):819–832. https://doi.org/10.1023/A:1006496308160

**Hnisz D, Shrinivas K, Young RA, Chakraborty AK, Sharp PA**. A phase separation model for transcriptional control. Cell. 2017:**169**(1):13–23. https://doi.org/10.1016/j.cell.2017.02.007

**Hoffmann G, Mahboubi A, Bente H, Garcia D, Hanson J, Hafr NA**. Arabidopsis RNA processing body components LSM1 and DCP5 aid in the evasion of translational repression during cauliflower mosaic virus infection. Plant Cell. 2022:**34**(8):3128–3147. https://doi.org/10.1093/plcell/koac132

**Hughes MP, Sawaya MR, Boyer DR, Goldschmidt L, Rodriguez JA, Cascio D, Chong L, Gonen T, Eisenberg DS**. Atomic structures of low-complexity protein segments reveal kinked beta sheets that assemble networks. Science. 2018:**359**(6376):698–701. https://doi.org/10.1126/science.aan6398

**Ivanov P, Kedersha N, Anderson P**. Stress granules and processing bodies in translational control. Cold Spring Harb Perspect Biol. 2019:**11**(5):a032813. https://doi.org/10.1101/cshperspect.a032813

**Jang GJ, Yang JY, Hsieh HL, Wu SH**. Processing bodies control the selective translation for optimal development of Arabidopsis young seedlings. Proc Natl Acad Sci U S A. 2019:**116**(13):6451–6456. https://doi.org/10.1073/pnas.1900084116

**Ji S, Luo Y, Cai Q, Cao Z, Zhao Y, Mei J, Li C, Xia P, Xie Z, Xia Z, et al.** LC domain-mediated coalescence is essential for Otu enzymatic activity to extend Drosophila lifespan. Mol Cell. 2019:**74**(2):363–377.e365. https://doi.org/10.1016/j.molcel.2019.02.004

**Johanson U, West J, Lister C, Michaels S, Amasino RM, Dean C**. Molecular analysis of FRIGIDA, a major determinant of natural variation in Arabidopsis flowering time. Science. 2000:**290**(5490):344–347. https://doi.org/10.1126/science.290.5490.344

**Kim EY, Wang L, Lei Z, Li H, Fan W, Cho J**. Ribosome stalling and SGS3 phase separation prime the epigenetic silencing of transposons. Nat Plants. 2021:**7**(3):303–309. https://doi.org/10.1038/s41477-021-00867-4

**Kroschwald S, Maharana S, Mateju D, Malinovska L, Nüske E, Poser I, Richter D, Alberti S**. Promiscuous interactions and protein disaggregases determine the material state of stress-inducible RNP granules. Elife. 2015:**4**:e06807. https://doi.org/10.7554/eLife.06807

**Li P, Tao Z, Dean C**. Phenotypic evolution through variation in splicing of the noncoding RNA COOLAIR. Genes Dev. 2015:**29**(7):696–701. https://doi.org/10.1101/gad.258814.115

**Lin Y, Protter DS, Rosen MK, Parker R**. Formation and maturation of phase-separated liquid droplets by RNA-binding proteins. Mol Cell. 2015:**60**(2):208–219. https://doi.org/10.1016/j.molcel.2015.08.018

**Liu Y, Du M, Deng L, Shen J, Fang M, Chen Q, Lu Y, Wang Q, Li C, Zhai Q**. MYC2 Regulates the termination of jasmonate signaling via an autoregulatory negative feedback loop. Plant Cell. 2019:**31**(1):106–127. https://doi.org/10.1105/tpc.18.00405

**Lu Y, Wu T, Gutman O, Lu H, Zhou Q, Henis YI, Luo K**. Phase separation of TAZ compartmentalizes the transcription machinery to promote gene expression. Nat Cell Biol. 2020:**22**(4):453–464. https://doi.org/10.1038/s41556-020-0485-0

**Luo Y, Na Z, Slavoff SA**. P-bodies: composition, properties, and functions. Biochemistry. 2018:**57**(17):2424–2431. https://doi.org/10.1021/acs.biochem.7b01162

**Macknight R, Bancroft I, Page T, Lister C, Schmidt R, Love K, Westphal L, Murphy G, Sherson S, Cobbett C, et al.** *FCA*, a gene controlling flowering time in Arabidopsis, encodes a protein containing RNA-binding domains. Cell. 1997:**89**(5):737–745. https://doi.org/10.1016/S0092-8674(00)80256-1

**Maldonado-Bonilla LD**. Composition and function of P bodies in *Arabidopsis thaliana*. Front Plant Sci. 2014:**5**:201. https://doi.org/10.3389/fpls.2014.00201

**Mittag T, Parker R**. Multiple modes of protein-protein interactions promote RNP granule assembly. J Mol Biol. 2018:**430**(23):4636–4649. https://doi.org/10.1016/j.jmb.2018.08.005

**Noda NN, Wang Z, Zhang H**. Liquid-liquid phase separation in autophagy. J Cell Biol. 2020:**219**(8):e202004062. https://doi.org/10.1083/jcb.202004062

**Patel A, Lee HO, Jawerth L, Maharana S, Jahnel M, Hein MY, Stoynov S, Mahamid J, Saha S, Franzmann TM, et al.** A liquid-to-solid phase transition of the ALS protein FUS accelerated by disease mutation. Cell. 2015:**162**(5):1066–1077. https://doi.org/10.1016/j.cell.2015.07.047

**Perea-Resa C, Hernández-Verdeja T, López-Cobollo R, del Mar Castellano M, Salinas J**. LSM Proteins provide accurate splicing and decay of selected transcripts to ensure normal Arabidopsis development. Plant Cell. 2012:**24**(12):4930–4947. https://doi.org/10.1105/tpc.112.103697

**Protter DSW, Parker R**. Principles and properties of stress granules. Trends Cell Biol. 2016:**26**(9):668–679. https://doi.org/10.1016/j.tcb.2016.05.004

**Sabari BR, Dall'Agnese A, Boija A, Klein IA, Coffey EL, Shrinivas K, Abraham BJ, Hannett NM, Zamudio AV, Manteiga JC, et al.** Coactivator condensation at super-enhancers links phase separation and gene control. Science. 2018:**361**(6400):eaar3958. https://doi.org/10.1126/science.aar3958

**Schomburg FM, Patton DA, Meinke DW, Amasino RM**. *FPA*, a gene involved in floral induction in Arabidopsis, encodes a protein containing RNA-recognition motifs. Plant Cell. 2001:**13**(6):1427–1436. https://doi.org/10.1105/TPC.010017

**Schütz S, Nöldeke ER, Sprangers R**. A synergistic network of interactions promotes the formation of in vitro processing bodies and protects mRNA against decapping. Nucleic Acids Res. 2017:**45**(11):6911–6922. https://doi.org/10.1093/nar/gkx353

**Shao W, Bi X, Pan Y, Gao B, Wu J, Yin Y, Liu Z, Peng M, Zhang W, Jiang X, et al.** Phase separation of RNA-binding protein promotes polymerase binding and transcription. Nat Chem Biol. 2022:**18**(1):70–80. https://doi.org/10.1038/s41589-021-00904-5

**Shindo C, Lister C, Crevillen P, Nordborg M, Dean C**. Variation in the epigenetic silencing of *FLC* contributes to natural variation in Arabidopsis vernalization response. Genes Dev. 2006:**20**(22): 3079–3083. https://doi.org/10.1101/gad.405306

**Simpson GG, Dijkwel PP, Quesada V, Henderson I, Dean C**. FY Is an RNA 3′ end-processing factor that interacts with FCA to control the Arabidopsis floral transition. Cell. 2003:**113**(6):777–787. https://doi.org/10.1016/S0092-8674(03)00425-2

**Tong J, Ren Z, Sun L, Zhou S, Yuan W, Hui Y, Ci D, Wang W, Fan LM, Wu Z, et al.** ALBA Proteins confer thermotolerance through stabilizing HSF messenger RNAs in cytoplasmic granules. Nat Plants. 2022:**8**(7):778–791. https://doi.org/10.1038/s41477-022-01175-1

**Wang Y, Tao Z, Wang W, Filiault D, Qiu C, Wang C, Wang H, Rehman S, Shi J, Zhang Y, et al.** Molecular variation in a functionally divergent homolog of FCA regulates flowering time in *Arabidopsis thaliana*. Nat Commun. 2020:**11**(1):e5830. https://doi.org/10.1038/s41467-020-19666-0

**Xie D, Chen M, Niu J, Wang L, Li Y, Fang X, Li P, Qi Y**. Phase separation of SERRATE drives dicing body assembly and promotes miRNA processing in Arabidopsis. Nat Cell Biol. 2020:**23**(1):32–39. https://doi.org/10.1038/s41556-020-00606-5

**Xu J, Chua NH**. Arabidopsis decapping 5 is required for mRNA decapping, P-body formation, and translational repression during postembryonic development. Plant Cell. 2009:**21**(10):3270–3279. https://doi.org/10.1105/tpc.109.070078

**Xu J, Chua NH**. Dehydration stress activates Arabidopsis MPK6 to signal DCP1 phosphorylation. EMBO J. 2012:**31**(8):1975–1784. https://doi.org/10.1038/emboj.2012.56

**Yoo SD, Cho YH, Sheen J**. Arabidopsis mesophyll protoplasts: a versatile cell system for transient gene expression analysis. Nat Protoc. 2007:**2**(7):1565–1572. https://doi.org/10.1038/nprot.2007.199

**Zavaliev R, Mohan R, Chen T, Dong X**. Formation of NPR1 condensates promotes cell survival during the plant immune response. Cell. 2020:**182**(5):1093–1108.e1018. https://doi.org/10.1016/j.cell.2020.07.016

**Zhang H, Li X, Song R, Zhan Z, Zhao F, Li Z, Jiang D**. Cap-binding complex assists RNA polymerase II transcription in plant salt stress response. Plant Cell Environ. 2022:**45**(9):2780–2793. https://doi.org/10.1111/pce.14388

**Zhang Y, Yang M, Duncan S, Yang X, Abdelhamid MAS, Huang L, Zhang H, Benfey PN, Waller ZAE, Ding Y**. G-quadruplex structures trigger RNA phase separation. Nucleic Acids Res. 2019:**47**(22): 11746–11754. https://doi.org/10.1093/nar/gkz978.

**Zhu P, Lister C, Dean C**. Cold-induced Arabidopsis FRIGIDA nuclear condensates for *FLC* repression. Nature. 2021:**599**(7886):657–661. https://doi.org/10.1038/s41586-021-04062-5